REPORT NO. NADC-89044-60
Contract No. N62269-86-C-0261

FATIGUE CRACK INITIATION MECHANICS OF METAL AIRCRAFT STRUCTURES

W. L. Morris, M. R. James, B. N. Cox
ROCKWELL INTERNATIONAL SCIENCE CENTER
1049 Camino Dos Rios
Thousand Oaks, CA 91360

AUGUST 1988

FINAL REPORT
PERIOD COVERING 1 AUGUST 1986 TO 10 OCTOBER 1987
Work Unit No. DG662B4
Program Element No. 61153N

Approved for Public Release; Distribution is Unlimited

Prepared for
Air Vehicle and Crew Systems Technology Department (Code 6043)
NAVAL AIR DEVELOPMENT CENTER
Warminster, Pa 18974-5000

NOTICES

REPORT NUMBERING SYSTEM - The numbering of technical project reports issued by the Naval Air Development Center is arranged for specific identification purposes. Each number consists of the Center acronym, the calendar year in which the number was assigned, the sequence number of the report within the specific calandar year, and the official 2-digit correspondence code of the Command Officer or the Functional Department responsible for the report. For example: Report No. NADC 88020-60 indicates the twentieth Center report for the year 1988 and prepared by the Air Vehicle and Crew Systems Technology Department. The numerical codes are as follows:

CODE	OFFICE OR DEPARTMENT
00	Commander, Naval Air Development Center
01	Technical Director, Naval Air Development Center
05	Computer Department
10	AntiSubmarine Warfare Systems Department
20	Tactical Air Systems Department
30	Warfare Systems Analysis Department
40	Communication Navigation Technology Department
50	Mission Avionics Technology Department
60	Air Vehicle & Crew Systems Technology Department
70	Systems & Software Technology Department
80	Engineering Support Group
90	Test & Evaluation Group

PRODUCT ENDORSEMENT - The discussion or instructions concerning commercial products herein do not constitute an endorsement by the Government nor do they convey or imply the license or right to use such products.

Unclassified
SECURITY CLASSIFICATION OF THIS PAGE

REPORT DOCUMENTATION PAGE

Form Approved
OMB No 0704-0188

1a REPORT SECURITY CLASSIFICATION Unclassified	1b RESTRICTIVE MARKINGS
2a SECURITY CLASSIFICATION AUTHORITY	3 DISTRIBUTION AVAILABILITY OF REPORT Approved for Public Release; Distribution is Unlimited
2b DECLASSIFICATION / DOWNGRADING SCHEDULE	
4. PERFORMING ORGANIZATION REPORT NUMBER(S) SC5470.FR	5 MONITORING ORGANIZATION REPORT NUMBER(S) NADC-89044-60
6a NAME OF PERFORMING ORGANIZATION ROCKWELL INTERNATIONAL SCIENCE CENTER 6b OFFICE SYMBOL (*If applicable*)	7a NAME OF MONITORING ORGANIZATION
6c ADDRESS (*City, State, and ZIP Code*) 1049 Camino Dos Rios Thousand Oaks, CA 91360	7b ADDRESS (*City, State, and ZIP Code*)
8a NAME OF FUNDING / SPONSORING ORGANIZATION Aircraft and Crew Systems Technology Department 8b OFFICE SYMBOL (*If applicable*) 6043	9 PROCUREMENT INSTRUMENT IDENTIFICATION NUMBER Contract No. N62269-86-C-0261
8c ADDRESS (*City, State, and ZIP Code*) NAVAL AIR DEVELOPMENT CENTER Warminster, PA 18974-5000	10 SOURCE OF FUNDING NUMBERS PROGRAM ELEMENT NO: 61153N PROJECT NO: TASK NO: R02303001 WORK UNIT ACCESSION NO: DG 662B4

11 TITLE (*Include Security Classification*)
Fatigue Crack Initiation Mechanics of Metal Aircraft Structures

12 PERSONAL AUTHOR(S)
Morris, W.L., James, M.R. and Cox, B.N.

13a TYPE OF REPORT	13b TIME COVERED	14 DATE OF REPORT (*Year, Month, Day*)	15 PAGE COUNT
Final Report	FROM 08/01/86 TO 10/10/87	1988 AUGUST	69

16 SUPPLEMENTARY NOTATION

17 COSATI CODES		
FIELD	GROUP	SUB-GROUP
11	06	01
20	11	

18 SUBJECT TERMS (*Continue on reverse if necessary and identify by block number*)
Fatigue; Crack Initiation; Slipband, Surface Layer, Aluminum Alloys

19 ABSTRACT (*Continue on reverse if necessary and identify by block number*)

The purpose of this research was to advance the understanding of deformation process that control the local stresses and strains at the grain size level in order to formulate a physically based model of crack initiation under spectrum loads. Experimental techniques of high spatial resolution strain measurements developed at the Science Center are used to investigate the mechanical behavior of individual constrained grains in Al 2219-T851. Local mechanical properties and yield criteria are deduced from measurements of the local-stress/strain hysteresis loop width. Two stages of flow are identified, each involving different yield locus behavior. Mathematical models of the local grain stiffness and the constrained plastic strain range are presented, and a phenomenological description of slip band nucleation and hardening are stated as functions of the local plastic strain range. These are then incorporated into a crack growth equation modified for plastic deformation to calculate the cycles required for a microcrack to reach the first subsurface grain boundary when propagating in a region of localized plastic flow. This provides a convenient engineering definition of crack initiation because it avoids the anomalous accelerated crack growth often found within the grain of initiation.

20 DISTRIBUTION AVAILABILITY OF ABSTRACT ■ UNCLASSIFIED/UNLIMITED ☐ SAME AS RPT ☐ DTIC USERS	21 ABSTRACT SECURITY CLASSIFICATION UNCLASSIFIED
22a NAME OF RESPONSIBLE INDIVIDUAL Dr. H.C. Tsai	22b TELEPHONE (*Include Area Code*) (215) 441-2871 22c OFFICE SYMBOL 6043

DD Form 1473, JUN 86 *Previous editions are obsolete*

S/N 0102-LF-014-6603

SECURITY CLASSIFICATION OF THIS PAGE
UNCLASSIFIED

TABLE OF CONTENTS

TABLE OF CONTENTS (continued)

LIST OF FIGURES

LIST OF FIGURES (continued)

NOMENCLATURE

Material Properties

D	Grain width
E_e	Elastic modulus
E_b	Contribution to plastic modulus in the grain from slip
E_{pg}	Plastic modulus in the grain
E_{pm}	Plastic modulus in the matrix surface layer
E_o&E_o'	Material parameters used to express E_{pg} in terms of matrix and slip components
γ	Crack growth rate exponent
γ_1, γ_2	Material parameters used to describe slip band activation
γ_3, γ_4	Material parameters used to describe slip band hardening
σ_y	Bulk 0.2% yield strength
σ_ℓ	Lower flow stress
σ_u	Upper flow stress

Constitutive Parameters

α_s	Constraint in the surface layer
α_g	Constraint in the grain
ϵ_p^g	Local plastic strain in the grain
$\Delta\epsilon_p^g$	Local plastic strain range in the grain
$\Delta\epsilon_p^m$	Local plastic strain range in the matrix surface layer
$\Delta\epsilon_p^I$	Plastic strain range for local initiation of slip bands
ϵ_r	Measured residual strain over one cycle
σ_g	Local stress in the grain

$\Delta\sigma_g$	Change in local stress in the grain
σ^a	Applied stress
σ^a_{max}	Maximum applied stress
σ^a_{min}	Minimum applied stress
ρ	Linear density of active slip bands
N	Fatigue cycles
n	Number of cycles to produce slip bands
n_s	Number of cycles in stress spectra (no plastic deformation)
n_p	Number of cycles in plastic strain spectra
η	Number of band nucleation sites/area of each type

Damage Parameters

a	Crack depth
Δa	Incremental crack depth growth
$\Delta\delta$	Crack tip opening displacement
ΔH	Incremental change in band hardening level
ΔI	Incremental change in band nucleation damage
m'	Number of blocks to nucleate a slip band
P( )	Probability distribution of damage parameters
ζ	Linear accumulation of damage
ΔK	Stress intensity range

Nomenclature in Papers

α	Constraint factor
E_p	Plastic modulus
E_e	Elastic modulus

$\Delta\epsilon_p$	Increment in plastic strain
σ	Applied stress
$\Delta\sigma$	Change in local stress
σ_{mean}	Mean stress
W_o	Width of applied stress-local strain hysteresis loop at zero load

1.0 INTRODUCTION

Conventional cumulative damage calculations based on macroscopic strain range work reasonably well for predicting the effect of load spectra on the fatigue lifetime of some alloys, especially steels.[1-3] These same procedures are notoriously inadequate for many other structural materials, including aluminum alloys. For aluminums, the reason the conventional analysis fails is known. The deformation that leads to cracking occurs in localized areas, i.e., individual grains, at the alloy surface.[4,5] Hence, the local stresses and strains differ substantially from the applied by amounts which depend on load sequence.

The purpose of the research under this one-year contract was to advance the understanding of the deformation processes that control the local stresses and strains in order to formulate a rational model of crack initiation under spectrum loads. Experimental techniques of high spatial resolution strain measurement developed at the Science Center were used to investigate the mechanical behavior of individual constrained grains in Al 2219-T851. Local mechanical properties and yield criteria can be deduced from measurements of the local stress-strain hysteresis loop width. Some of our recent findings have changed the structure of the model initially envisaged for the Al 2219-T851 material studied:

1. Fatigue-induced lowering of the local yield strength in isolated microplastic grains in Al 2219-T851 is <u>not</u> the result of a change in flow stress. Instead, the plastic modulus of the grains decreases progressively with fatigue.[6] A distribution in the strain range required for slip band nucleation is needed to explain the load history/stress amplitude dependence of grain softening.

2. The decrease in stress/strain loop width seen in grains later in lifetime results from strain hardening. Further, if individual grains are completely hardened at one cyclic stress, they will revert to a softened state if the cyclic stress is raised. The hardening rate is faster in grains in which the local plastic strain is large. Hardening is probably not due

to cross slip, but rather to cumulative damage in each slip band that ultimately deactivates slip in the band.

3. The two stages of flow found in Al 2219-T851 involve different constitutive relationships.[4,5,7] The high strain hardening flow at small stresses is kinematic[4] and we believe this occurs in Al 2219-T851 in a thin layer at the surface. A kinematic behavior could imply that there exists a short range internal constraint of the deformation which creates a local back stress.

4. Flow above the upper flow stress in Al 2219-T851 is stationary, suggestive of unimpeded deformation until the slip bands reach the grain boundaries. A model of the stress-strain behavior of the two flow stress systems has been proposed by viewing the material as a microscopic composite.[7]

5. Consistent with the picture that softening involves the creation of slip bands in a surface layer, which then penetrate the grain body, is the finding that all Al 2219-T851 grains soften, but that the initial strains in large grains are much larger than in smaller grains.

6. A convenient engineering definition of crack initiation in Al 2219-T851 is shown to be the cycles required for the localized plastic flow in a grain to assist microcrack propagation to the first subsurface grain boundary.

In the next section, we discuss these findings. We then proceed to a description of a lifetime initiation model which supposes a microscopic inhomogeneity of the deformation of individual Al 2219-T851 grains to obtain expressions to calculate the locally evolving mechanical properties and the resulting crack initiation rates. This model is phenomenological. It replaces several areas of analysis where mechanistic insight is still lacking with empirical expressions that can now be directly calibrated with microscopically measured deformation parameters. Perhaps in the future, calibration can be indirect through lifetime response to standardized load sequences.

2.0 OBSERVATIONS ON LOCAL DEFORMATION IN Al 2219-T851

Questions raised in our initial proposal were the following:

1. Is the slip band model[8] we had proposed (under NSF contract) for grain softening correct?

   Results in the paper presented in Section 2.1 indicate that some of the essential features of the deformation are correctly predicted. For example, softening is associated with a decreasing plastic modulus, as expected when the slip band density increases. The fine details are different from that originally imagined, however. For instance, deformation below the upper flow stress σ_U strain hardens with fatigue, possibly because the slip bands reduce the volume of the surface layer which can deform. To describe the softening rate vs local strain range, we propose an empirical model (Section 2.3) requiring calibration by microscopic deformation measurements.

2. Does deformation associated with each of the two separate flow stresses in Al 2219-T851 obey the same yield locus behavior?

   No. As described in the paper presented in Section 2.2, deformation between the lower flow stress, σ_ℓ and σ_U, the upper flow stress, is kinematic. Above σ_U, the deformation flow criterion is stationary. This is a further confirmation that flow below σ_U is localized in the grain matrix, and above σ_U occurs in long ranged bands which reach the grain boundaries.

3. Can we ignore the local hardening?

   It could be seriously over-conservative to do so. For high stress amplitudes near yield, correction for hardening cannot matter because crack

initiation occurs in the large grains before they have time to harden. But, at lower amplitudes, the much slower rate of hardening in some smaller grains makes them the potential cracking targets, in comparison to the very large grains which are protected from cracking by hardening. (See Section 2.3 for discussion.)

4. What is an appropriate initiation lifetime criterion?

   We have decided on equating initiation lifetime with the cycles to form a grain sized crack. Our reasoning is discussed in Section 2.3.

5. Finally, how can one simplify the complexities of nature sufficiently in a model to allow lifetime to be predicted under spectrum loading?

   At first, we thought that it might suffice to model what happens only in the largest grains. But now this is clearly inadequate. We have therefore designed an initiation lifetime model that accounts for grain size effects. Its format is such that important stochastic elements and perhaps even a probabilistic formulation of the model could be made in the future. (See Section 4 for details.)

2.1 Mechanical Property Evaluation

In two previous papers,[4,5] we used models of the deformation of a soft ellipsoid in an elastic matrix to calculate the flow stress and strain hardening characteristics of surface grains in Al 2219-T851. We found that fatigue of Al 2219-T851 at stresses below the bulk cyclic yield strength caused a reduction in the local 0.2% offset yield strength of the interior of the grains. Grains 3-8 times larger than the 60 μm mean size were the most affected and are the eventual sites for crack initiation. Ultimately, the yield strength of these grains falls to half the bulk cyclic value. However, the local strain amplitude remains small because the deformation is constrained by the surrounding nearly elastic grains.

To provide more experimental evidence for this fatigued induced reduction in the local flow stress, we used a load reduction sequence to minimize the influence of local residual stresses. This technique was used to characterize the evolution of the flow stress in a 300 μm grain in Al 2219-T851. The results were published in Fatigue 87 (3rd Int. Conf. on Fatigue and Fatigue Thresholds) (Ref. 6) and are included as Appendix A. In summary, two flow stresses were identified. Microplastic flow takes place in all grains at fully reversed stress amplitudes above 70 MPa, although the plastic modulus is large and only small amounts of plastic deformation occur. With continued fatigue, an upper flow stress develops at ~ 200 MPa in grains substantially larger than the mean grain size. In these grains, plastic flow is easier and considerable plastic strain occurs. This suggests the existence of matrix slip (which occurs above the lower flow stress) penetrated by slip bands (which occurs above the upper flow stress). The deformation behavior of the grain might be explained then by a composite model incorporating two deformation regimes.

2.2 Yield Locus Motion During Spectrum Loading

The behavior of the two stages of flow identified in Al 2219-T851 was investigated in more detail in order to accurately describe the deformation pattern by a composite model. Various load sequences were used since prior to this, all our studies had been done using only fully reversed loading. Two limiting cases of the flow surface locus were examined by studying the response to several load sequences. These were the stationary locus, wherein the flow stress is independent of prior load, and the kinematic surface, in which the flow stress moves freely with the maximum stress excursion on the previous load reversal. This effort was reported at the Symposium on Effects of Load and Thermal Histories on Mechanical Behavior of Metals[7] and is included as Appendix B.

In summary, flow above the lower flow stress was found to strain harden quickly and is best described by kinematic movement of the flow surface. This suggests there is considerable reaction to short range back stresses in the grain, and deformation is extremely dependent on the prior load sequence. Deformation above the upper flow stress shows strong strain softening with fatigue and is best described by a stationary yield locus. This is consistent with long range flow constrained by grain boundaries, such as in coarse slip bands. A physical representation of this behavior is that of a matrix containing slip bands. A uniform deformation model incorporating both of these kinds of behavior was developed which provided an adequate description of deformation in the isolated grains responsible for crack initiation.

2.3 Observations Bearing on Slip Band Formation, Hardening and the Crack Initiation Criterion

Several years ago we showed, for Al 2219-T851 in fully reversed loading, that low amplitude cycles hardened the surface.[9] This reduced the subsequent initiation of cracks once the cyclic stress was raised. The model we proposed at the time related a hardening rate to the local plastic strain range. In light of our most recent findings, however, the resulting expression for evolution in the plastic strain range cannot be correct, although the disparity with reality might be difficult to notice if the load spectra is not complex. The old model in effect assumed that the grain hardening was caused by cross-slip which interdicted the active bands. With sufficient fatigue, the model equations predicted that a grain would fully harden at any cyclic stress. New measurements of strains in individual grains show this picture is inaccurate. What actually happens is that raising the stress after hardening causes a new round of softening, although producing plastic strain amplitudes lower than would be expected (Fig. 2.3-1) if one had begun fatigue with the higher cyclic stress. Presumably, therefore, it is only the slip bands formed at the low amplitude which harden. Apparently, there is a distribution in the local matrix strain range required for band nucleation, and a critical strain range must be exceeded to produce an active band at each potential band nucleation site.

How can we relate the local strain range in the matrix and the strain range required for development of a band at each potential nucleation site in a surface layer to the number of cycles required to form a band? Clearly, there is insufficient information about the microscopic mechanisms to do this exactly, so we make the following rationalization. For Al 2219-T851, the fatigue limit in fully reversed loading is ≈ ±50% of the bulk cyclic yield strength. We assume that the plastic matrix strains corresponding to this stress range are just of sufficient magnitude to produce slip bands. For applied stresses greater than ±50% of yield, the number of cycles (N) to produce bands is obtained from plots of the local residual strain vs cycles, such as Fig. 2.3-1. The cycles to produce a band at a site requiring the maximum applied cyclic strain is assumed to correspond to the cycles to reach the maximum plastic strain amplitude. (Because each grain cyclically hardens, this procedure probably underestimates N, i.e., it is conservative.) The cycles to produce bands at sites capable of forming bands at 50% of

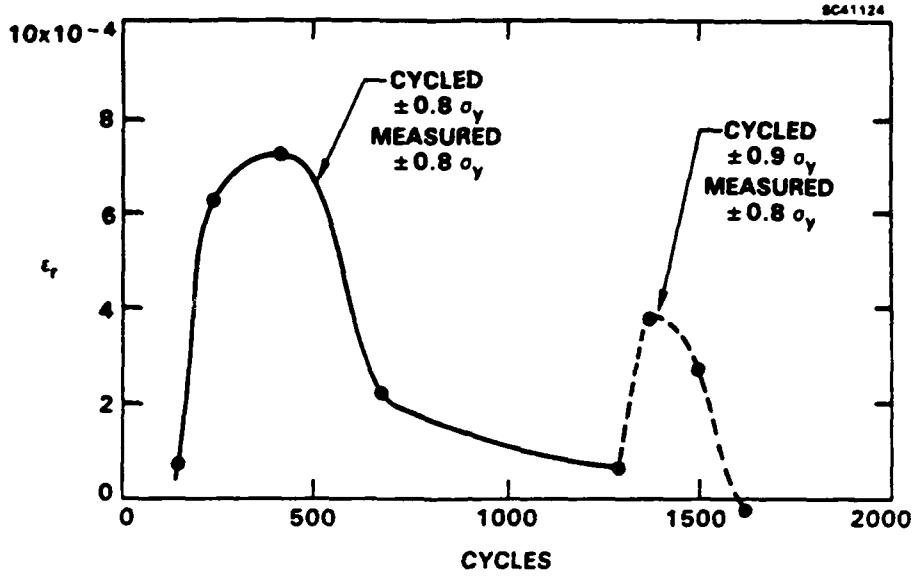

Fig. 2.3-1 Residual strain measured in a 300 μm grain after tensile loading. Specimen first cycled until hardened at ±0.8 σ_y, then subjected to ±0.9 σ_y. [σ_y is bulk yield strength.]

yield, when the applied stress is greater than 50%, is read as the cycles where the onset of a positive residual strain begins. From Fig. 2.3-1, N ≈ 150 cycles at ±0.8 σ_y.

We propose an accumulative damage model to predict the cycles to form each slip band. This is calibrated for constant stress amplitude (and quasi constant local matrix strain amplitude) loading.

Imagine that a grain experiences a local plastic strain range $\Delta\varepsilon_p^m$ in the matrix. The total measureable strain increases with fatigue as slip bands form, until the band initiation process stops. At this point, the range $\Delta\varepsilon_p^m$ has activated all bands requiring an activation strain range, $\Delta\varepsilon_p^I$, which is less than the plastic strain in the matrix, $\Delta\varepsilon_p^m$. No further bands can be activated unless $\Delta\varepsilon_p^m$ is increased.

However, before this point is reached, all sites requiring activation strains $\Delta\varepsilon_p^I < \Delta\varepsilon_p^m$ have produced bands. A simple construction described below allows us to estimate the number of constant amplitude cycles this takes. Later on, as we develop the spectrum loading model, the reciprocal of these cycles (Eq. 2.3-2) will be the damage rate for the local plastic strain range $\Delta\varepsilon_p^m$.

We can use an expression for the local fully reversed plastic strain range in a kinematic domain (the matrix surface layer denoted by m) embedded in the grain to relate the strain range to σ_g, the local stress excursion in the grain.

$$\Delta\varepsilon_p^m = \frac{2(\sigma_g - \sigma_\ell)}{E_{pm} + \alpha E_e} . \qquad (2.3\text{-}1)$$

σ_ℓ has already been defined as the lower flow stress, E_{pm} is the plastic modulus in the surface layer, α is a shape factor constant and E_e is Young's modulus. This allows us to make the construction in Fig. 2.3-2. The symbols represent data points from experiments where the cycles required for the local stress to exceed σ_ℓ and σ_u were obtained at four different applied stress levels. Once the local stress exceeds σ_u, the plastic strain in the matrix, $\Delta\varepsilon_p^m$, exceeds that for activation of slip bands. The solid line in Fig. 2.3-2 is fit through the second of each pair of data points taken at different applied stress amplitudes. This line relates the critical plastic strain necessary to activate all slip bands to cycles. Some slip bands activate at a lower strain down to that reached when σ_ℓ is exceeded, as denoted by the lower data point of each pair. The dashed line connecting the pair of experimental data points to the origin can then be used to calculate the cycles required to form a band at a site requiring a lower activation plastic strain than the applied. Call $\Delta\varepsilon_p^I$ the local range for band activation and the cycles to band formation seen in Fig. 2.3-2 has the form

$$n = \frac{\Delta\varepsilon_p^I}{\Delta\varepsilon_p^m} 10^{\frac{\gamma_1 - \Delta\varepsilon_p^m}{\gamma_2}} . \qquad (2.3\text{-}2)$$

γ_1 and γ_2 are material parameters determinable by fitting Eq. (2.3-2) to the data in Fig. 2.3-2. We have noted earlier in this report that deformation below σ_u, the upper flow stress, is kinematic and is therefore in the matrix penetrated by bands. As such, the local deformation is short ranged and can "feel" the presence of grain boundaries only through a reaction stress to the net plastic strain. Thus, n in Eq. (2.3-2) is independent of grain size.

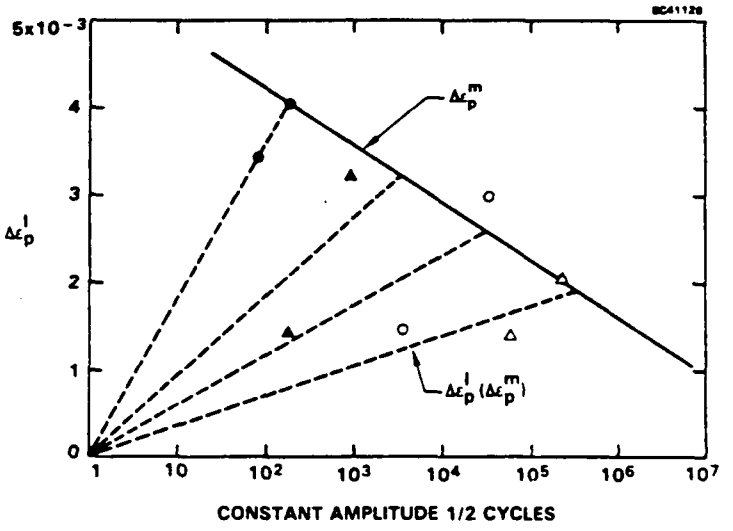

Fig. 2.3-2 Relationship of cycles to band initiation to $\Delta\varepsilon_p^m$ and $\Delta\varepsilon_p^I$ for fully reversed loading. The dashed lines represent families of critical plastic strain to band activation at constant plastic strain in the matrix surface layer.

However, this does not mean that the strains measured in each grain will be independent of grain size. Observations made under a prior contract[10] with NADC have led to the hypothesis that, in Al 2219-T851, slip is initiated in a thin layer near the surface. The number of band nucleation sites in each grain will, therefore, be proportional to the grain width (D) and the band displacements per unit length will be proportional to D, giving $\Delta\varepsilon_p^m \propto D^2$.

Such a trend has been verified for Al 2219-T851 using data acquired several years ago (Fig. 2.3-3). Additionally, another set of residual strains in 150 and 300 μm grains have been determined for Al 2219-T851. These were taken after several hundred cycles and also confirm trend with grain size shown in Fig. 2.3-3. So, the interiors of all the surface grains apparently soften at the same rate in terms of bands produced per site available, but the grain size affects the magnitude of the strains which result.

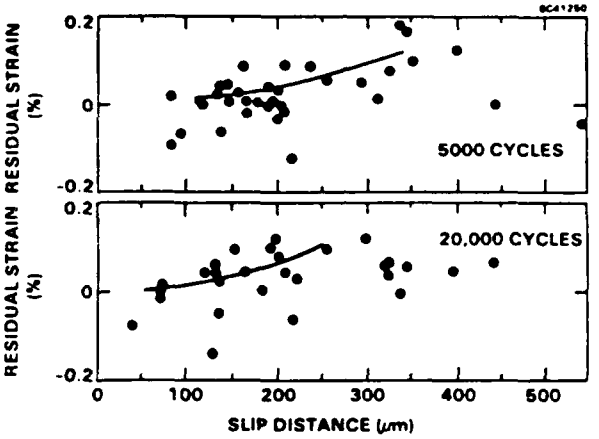

Fig. 2.3-3 Effect of grain size on measured residual strain. Data from Ref. 9 for ±270 MPa cycles in Al 2219-T851. Residual strains measured after a tensile load. Curves are proportional to D^2 and fit the data for grains small enough to be essentially unhardened.

The other important effect of grain size appears in the grain hardening rate. We think this is because the displacements experienced by individual bands increase with grain size. Large grains harden much faster than small grains. Also, there is a pronounced effect of applied strain range on the rate of hardening of individual grains (Fig. 2.3-4). The hardening rate decreases markedly as the cyclic stress is lowered. Because the displacement of individual bands should be proportional to $(\Delta\sigma_g - 2\sigma_u)D$ in fully reversed loading, there should be a correlation of this quantity to the cycles for band hardening. We use the number of constant amplitude cycles it takes the locally measured residual strain to fall to ≈ 1/e of its maximum value to obtain an empirical relationship of the cycles to harden a band as a function of the grain size and load (Fig. 2.3-5). In fully reversed loading,

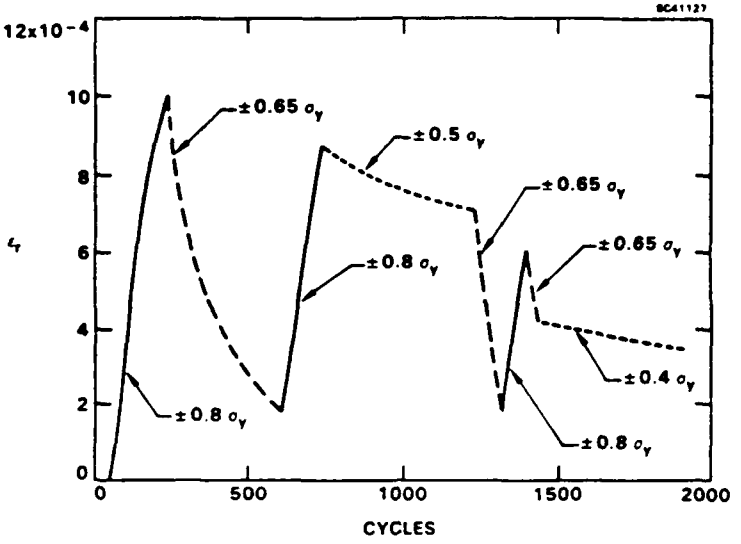

Fig. 2.3-4 Effect of loading range on hardening of residual strains ϵ_r measured in a 300 μm grain. Compare to Fig. 2.3-1 where hardening at constant amplitude is almost complete by 600 cycles.

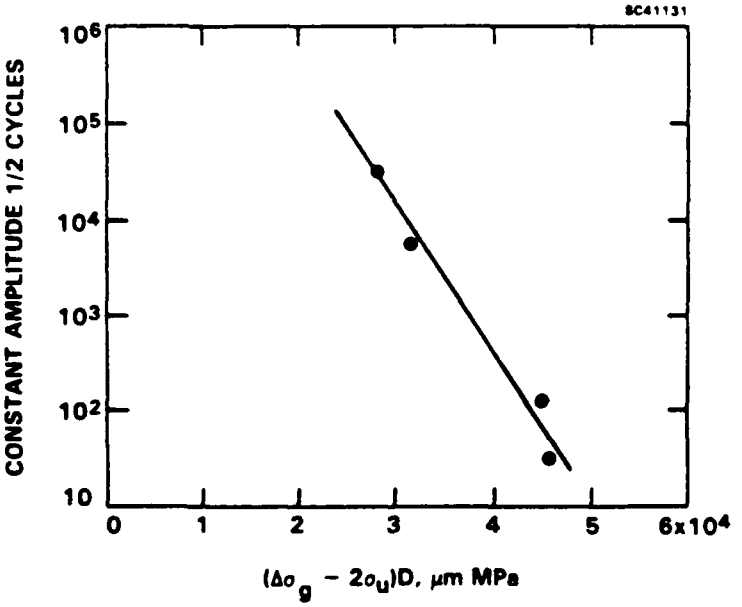

Fig. 2.3-5 Empirical relationship of estimated cycles to fall to ≈ 1/e of the maximum local residual strain and the quantity $(\Delta\sigma_g - 2\sigma_u)D$.

$$N = 10^{\gamma_3}\, 10^{(-\gamma_4(\Delta\sigma_g - 2\sigma_u)D)} \qquad (2.3\text{-}3)$$

expresses the relationship in Fig. 2-3.5. The γ's are constants determinable for Al 2219-T851 from Fig. 2.3-5. Once a band forms, it presumably forgets the $\Delta\varepsilon_p^I$ of its initiation site, and only the strains to which it is exposed after it forms and their duration control its hardening state.

We now discuss our rationale for defining crack initiation as the cycles to obtain a crack of one grain depth. Experiments we did several years ago[9] showed a strong correlation between the peak local plastic strain in a grain and constituent particle fracture. However, those grains which deformed extensively also accumulated large cycle-by-cycle damage levels, casting doubt as to the true initiation mechanism, i.e., peak strain or accumulated damage. Furthermore, for this study, there was the need of a deformation model of initiation with sufficient practical engineering significance to formulate a lifetime model. Since single extreme overloads can fracture constituent particles in Al 2219-T851, but not propagate the crack into the grain, a peak strain criterion describing this behavior seemed of no practical importance. However, early crack growth to the first grain boundary comprises a phenomena common to many alloys, including Al 2219-T851, which is also a type of "initiation" and can be a primary factor in controlling lifetime. Our modeling of local plasticity provides for the first time the opportunity to predict this "initiation life".

For 15 years, it has been recognized that very short surface cracks propagate faster than long cracks at the same cyclic stress intensity.[11-12] After corrections have been made for closure stress and its dependence on crack length, and for crack growth statistics affected by local microstructure, one finds that the very shortest cracks (perhaps smaller than 25 μm) still grow much too fast to be understood by linear elastic fracture mechanics. Lankford et al,[13] Smith[14] and Miller[15] have attributed this accelerated growth to an enhanced crack tip plasticity, perhaps predictable by a second order term in the expression for stress intensity. However, for very short cracks, these stress intensity corrections still grossly underestimate the actual growth rates. This, we

believe, is because these models presume that the surface is otherwise elastic, while it is clearly not in many materials. In prior work,[17] we found that by using the elastic-plastic crack growth expression by Tompkins,[16] we obtained from known plastic strains in a grain at a crack tip an estimate of the true crack tip opening displacement (CTOD) for cracks 50 μm and larger. It was typically a factor of two larger than anticipated for an elastic medium. It was the long-range plastic strains induced not by the crack itself, but by the independent deformation of the grain surrounding the crack which increased the CTOD and accelerated growth.[17]

Further analysis now shows that the relatively small correction to CTOD provided by the Tompkins expression may produce several orders of magnitude increase in growth rate to a microcrack smaller than 20 μm, the typical size of the largest intermetallic in Al 2219-T851. The key in predicting growth rate is to accurately know the local plastic strain range cycle-by-cycle. In all likelihood, as long as the entire crack is embedded in the plastic strain field of a surface grain, it will feel the accelerating effect of this plasticity. Once a crack begins to pass below the first subsurface grain boundary, the growth rate should start to converge towards an LEFM prediction. This association was noted by Lankford[18] some years ago, but the reason why it existed was mystifying. Under this contract, we have measured strains on the surface just in front of a growing 15 μm crack and confirm that the grain must be softer for there to be substantial enhancement propagation in Al 2219-T851.

This simple definition of initiation, as the number of cycles required to initiate and propagate a microcrack to the first subsurface grain boundary, has satisfying engineering applications. The arrival of the crack front at the subsurface grain boundary corresponds to the point in lifetime beyond which LEFM suffices to give a crude estimate of the life remaining (although corrections for effects of the microstructure on the small crack growth would still be advisable). This is not to be considered a universal definition of "initiation," but it should apply to many high-strength aluminum alloys.

3.0 APPARENT "INITIATION" LIFETIME SCENARIO

Individual grains develop slip bands, whose presence strain softens the local surface, accelerating crack initiation. In Al 2219-T851, the bands are thought to nucleate at sites scattered within a thin (≈ 2 μm deep) surface layer,[5] as illustrated in Fig. 3.0-1. For a fully reversed local plastic strain in the layer, damage leading to band nucleation accumulates faster the larger the strain $\Delta\varepsilon_p^m$ and the smaller the activation strain range ($\Delta\varepsilon_p^I$) for each site. $\Delta\varepsilon_p^m$ must be greater than or equal to $\Delta\varepsilon_p^I$ for a band to ultimately form by fatigue. A phenomological model for the rate of band initiation vs $\Delta\varepsilon_p^m$ and $\Delta\varepsilon_p^I$ has been proposed in Section 2.3 for Al 2219-T851, based upon microscopic strain observations. Since deformation of the surface layer is kinematic, there can be no direct effect of grain size on $\Delta\varepsilon_p^m$. However, the layer size affects the number of slip bands that can form, since larger grains will have more potential nucleation sites/length. Also, the coupling between grain size, band density and elastic modulus in the grain body will affect the local stress range which controls $\Delta\varepsilon_p^m$.

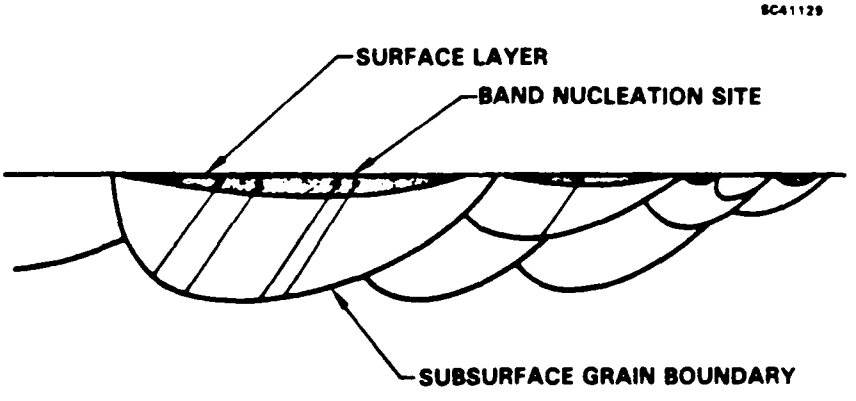

Fig. 3.0-1 Schematic cross-section of a grain showing bands that have nucleated at sites in a thin surface layer.

To find $\Delta\varepsilon_p^m$ and the plastic strain range in the grain body $\Delta\varepsilon_p^g$, it is necessary to make a parallel calculation of the deformations in the grain body vs band density, as well as in the surface layer. For economy of numerical analysis, the load spectrum will be subdivided into repetitive blocks.

3.1 Surface Layer - Nucleated Band Density

An incremental change in damage at a potential band nucleation site over a loading block is defined to be $\Delta I(E_{pg}, \Delta\varepsilon_p^I)$. [Naturally, ΔI also depends upon the load spectra comprising the block.] E_{pg} is the plastic modulus of the entire grain. Summed over repeated blocks, the requirement for initiation of a band at a site of initiation range $\Delta\varepsilon_p^I$ is

$$I(\Delta\varepsilon_p^I) = 1 \, . \tag{3.1-1}$$

After m blocks, there exists a maximum activation strain of the sites which have produced slip bands. We call this quantity $\Delta\varepsilon_p^{I_{max}}$, and it is found by solving Eq. (3.1-1).

If no strain hardening has occurred during m blocks, the linear density of active slip bands ρ in a grain of width D would simply be

$$\rho = D \int_0^{\Delta\varepsilon_p^{I_{max}}} n(\Delta\varepsilon_p^I) d\Delta\varepsilon_p^I \, . \tag{3.1-2}$$

$n(\Delta\varepsilon_p^I)$ is the number of band nucleation sites/area of each type.

3.2 Grain Body

Under stress, each active band will displace an amount proportional to its width. The apparent plastic modulus of the grain becomes

$$E_b = \frac{E_o}{D^2 \int_0^{\Delta\varepsilon_p^{I_{max}}} n(\Delta\varepsilon_p^I) \, d\Delta\varepsilon_p^I} \, . \tag{3.2-1a}$$

$$E_{pg} = \frac{E_o' E_b}{E_o' + E_b}, \qquad (3.2\text{-}1b)$$

where E_o and E_o' are material parameters.

E_{pg} is an effective modulus, i.e., an average of the composite caused by plastic flow of the matrix and slip of any active bands present. When there are no bands, $E_b \to \infty$ and $E_{pg} = E_o'$, which must therefore be the plastic modulus of the matrix, i.e., $E_o' = E_{pm}$. Parameter E_o can be determined by calibration once Eq. (3.2-1a) is calculable. This requires a determination of $E_{pg}(n)$ as described in Sect. 2.2 (defined as Ep(i) in the paper) for comparison to Eq. 3.2-1b through the application of Eqs. 3.2-1a and 2.3-2. Since E_o is a fundamental material parameter, this analysis needs to be done just once for each material modeled.

When a spectrum load is applied, the local stress in the grain's main body σ_g differs from the applied σ^a by a residual stress which is proportional to the local plastic strain in the grain (ε_p^g). The stress-strain behavior is calculated by a "stationary" flow criterion, which treats a single flow stress σ_u of the active bands as invariant. Softening in this model is the result of a progressive reduction in E_{pg} as $\Delta\varepsilon_p^{I_{max}}$ increases.

Strain hardening is handled by considering the deformation of each slip band. We assume in accord with the experiment that each new band will slip on exceeding σ_u until it has accumulated a hardening level between m' (nucleation) and blocks

$$\Delta H_{m',m} = 1. \qquad (3.2\text{-}2)$$

The cycles to reach this critical $\Delta H_{m',m}$ will depend upon grain size because the cycle-by-cycle strain in each individual band increases with grain size for a constant E_{pg}.

We define an incremental hardening $\Delta H(E_{pg}, D)$ for one loading block, determined by microscopic observations. (E_{pg} and ρ depends upon D.) ΔH is summed block-by-block to determine $\Delta H_{m',m}$ and thus how long it takes a newly formed band to

cease slipping. Once a band forms, it apparently loses all memory of its origin other than "when" it formed. All bands nucleated at m' blocks will therefore, in this model, cease to slip at the same time in the future. So, the density of active slip bands (ρ) can be expressed by a simple integral of η.

$$\rho = D \int_{\Delta\varepsilon_p}^{\Delta\varepsilon_p^{I_{max}}} \eta(\Delta\varepsilon_p^I)\, d\Delta\varepsilon_p^I \,. \tag{3.2-3}$$

where $\Delta\varepsilon_p^{I_{min}} = \Delta\varepsilon_p^{I_{max}}(m')$: and (3.2-4)

m' is obtained by solving

$$H(m) - H(m') = 1. \tag{3.2-5}$$

Wherefore

$$E_b = \frac{E_o}{D^2 \int_{\Delta\varepsilon_p}^{\Delta\varepsilon_p^{I_{max}}} \eta(\Delta\varepsilon_p^I)\, d\Delta\varepsilon_p^I} \,, \tag{3.2-6a}$$

$$E_{pg} = \frac{E_o' E_b}{E_o' + E_b} \,. \tag{3.2-6b}$$

Consequently, grain hardening with fatigue in this model is tied to a progressive increase in $\Delta\varepsilon_p^{I_{min}}$, the minimum plastic strain range capable of initiating a slip band, and the resulting increase in E_{pg}.

3.3 Crack "Initiation"

First, we must calculate E_{pg} and the associated σ_g and ε_p^g cycle-by-cycle.

These stresses and strains control initiation. As a practical matter, the smallest cracks that are routinely found in laboratory specimens in structural aluminums are typically one-grain thickness in depth. Since local plasticity in a surface grain greatly accelerates growth, a grain-sized crack corresponds to the smallest crack size for which simple microstructual-based corrections to linear elastic fracture mechanics provide an adequate expression for growth rate. Also, the average growth rate is a minimum at one-grain depth (Fig. 3.3-1).

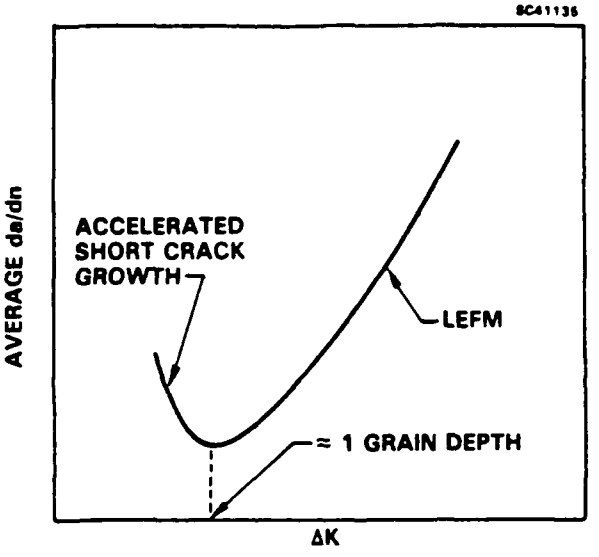

Fig. 3.3-1 Typical dependence of average short crack growth rate on ΔK.

Plastic strains can accelerate growth in the first grain by a factor of 100. So, a definition of "initiation" as corresponding to one-grain depth has fundamental physical and engineering significance. In the following, we show how our current insight on local plasticity can be incorporated into an elastic-plastic growth equation of Tompkins[16] (see Section 4.1.7) to predict "initiation" under spectrum loads. We distinguish Mode I crack growth initiating from intermetallic particles and mixed mode growth from slip bands, so that the model should be suitable for most high strength aluminum alloys having these crack initiation modes.

4.0 OVERALL MATHEMATICAL STRUCTURE

The cycles to initiation $(mn)_I$ [# of blocks times # cycles in block] will depend on the local grain size. The grain size leading to earliest initiation will vary with the load spectrum. Brute force numerical simulations of initiation must therefore be replaced with a mathematics of the initiation process suitable for solution by numerical techniques. The numerical coding of the response functions needed to exercise this model is left to the reader. In the following, the model is stated in detail only for initiation with mode I growth from constituent particles.

Because the rate at which the local mechanical properties change depends on grain size, we cannot a priori tell which local grain size in an alloy will lead to earliest initiation. In fact, it is certain that this critical size will depend upon load sequence. The trend will be for large grains which can sustain layer plastic strains to advance a microcrack most rapidly from a fractured intermetallic. However, large grains are also more subject to strain hardening, so they may only actively deform for a short time, leaving the job of producing the terminal crack to a grain of more modest size. In the following, we define a set of damage functions which depend on grain size. The numerical concept is to determine these functions for block-by-block loading, so that the grain size dependence of the incremental crack growth is automatically contained in each intermediate result. The calculation can be carried out until the crack depth within the range in grain sizes reaches a critical size. The calculation does not follow the evolution of damage of single grains, but rather describes the evolution of a damage state space in which grain size is a variable.

Four levels of analysis are identified. At level 1 are three individual loading block response functions in which the response of any surface grain is embedded, at any time during fatigue, to one standard loading block. The parameters represented will allow the progressive evolution of the local mechanical properties to be predicted, from which the incremental change in crack length of a subgrain-sized crack can be estimated block-by-block.

The functions are:

$\Delta I(E_{pg}, \Delta\varepsilon_p^I)$;	incremental damage for band nucleation
$\Delta H(E_{pg}, D)$;	incremental damage for band hardening
$\Delta a(E_{pg}, a)$;	incremental growth of a subgrain sized crack of depth a

The new variable here is (a), the crack depth. The way these functions serve the initiation lifetime calculation is illustrated schematically in Fig. 4.0-1.

Once these three functions have been determined, a simulation of the initiation process can proceed. The functions will be used as "look up" tables for values needed in this sequential analysis.

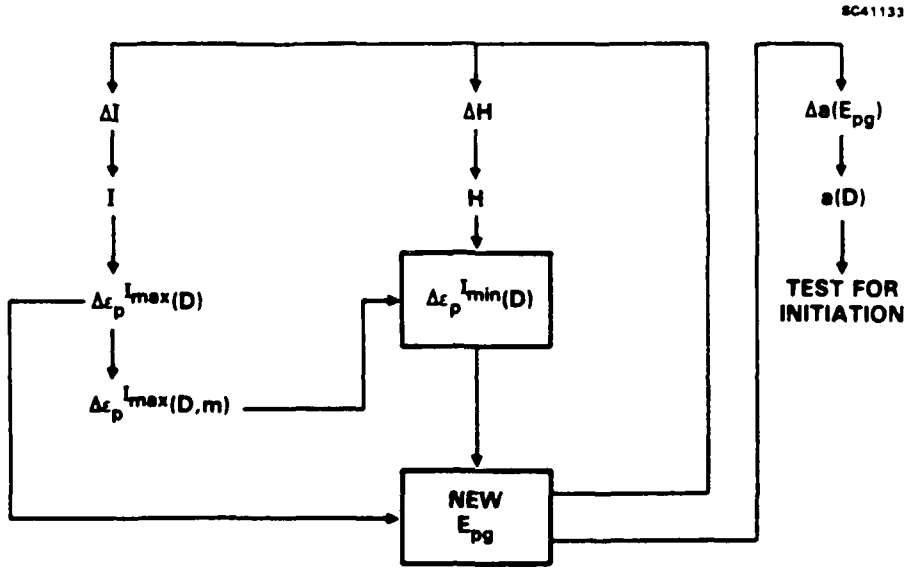

Fig. 4.0-1 Block-by-block calculation of crack length.

At level 2 are functions which must be determined and stored only to the next loading block. These are

$I(D, \Delta\varepsilon_p^I)$;	the cumulative damage for initiation of a band at a $\Delta\varepsilon_p^I$ activation site in a grain of size D
$a(D)$;	the crack depth vs D
$\Delta\varepsilon_p^{I_{max}}(D)$;	the maximum $\Delta\varepsilon_p^I$ which has caused band nucleation
$\Delta H(D)$;	the incremental hardening vs grain size

Two level 3 functions retain a running memory from the first block of the cumulative damage governing band density. These are necessary to calculate the mechanical property state for each succeeding block.

$\Delta\varepsilon_p^{I_{max}}(D,m)$;	is a running value of $\Delta\varepsilon_p^{I_{max}}(D)$
$H(D,m)$;	is the summed hardening coefficient

The final level 4 contains

$\Delta\varepsilon_p^{I_{min}}(D)$;	the minimum $\Delta\varepsilon_p^I$ for which bands have ceased to slip
E_{pg};	the plastic modulus of the grain's main body
$\rho(D)$;	the active slip band density

Some reasonable mixture of microscopic data on local strains and fatigue test data will be needed to calibrate this model. The following is just one of several options.

4.1 The Loading Block Response Functions

The spectrum loading block must first be expressed in terms of sequential minimum and maximum applied stresses σ^a_{min} and σ^a_{max}. For a selected E_{pg}, these are used to find the local stress σ_g and plastic strain ε^g_p in the grain body. σ_g is then used as an effective applied stress to find $\Delta\varepsilon^m_p$ in the surface layer embedded within the grain. With appropriate rain flow sequence counting[19] $\Delta\varepsilon^g_p$ and $\Delta\sigma_g$ give Δa, $\Delta\sigma_g$ is used to find ΔH, and $\Delta\varepsilon^m_p$ is used along with $E_{pg}(D)$ to find ΔI. See Fig. 4.1-1 for the logic of this procedure.

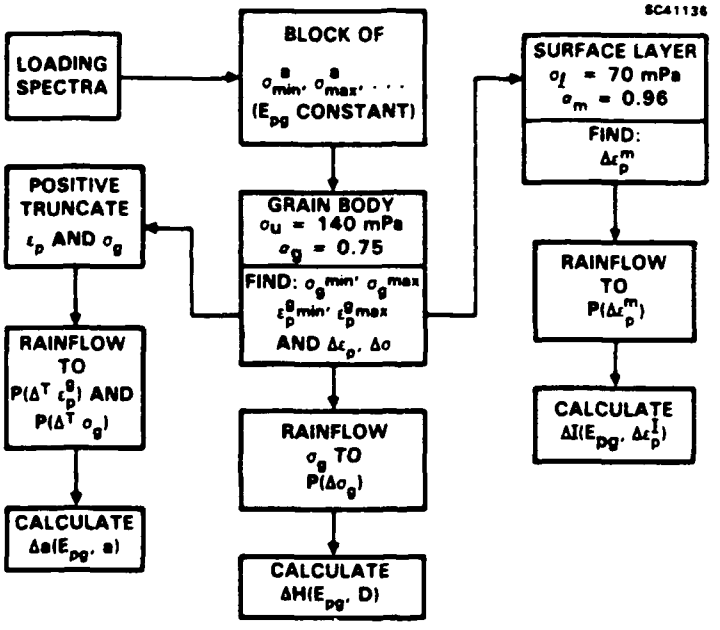

Fig. 4.1-1 Calculating the loading block response functions.

Note: The calculation described is of an average initiation lifetime. Variability in constraint (α_s and α_g for the surface layer and grain, respectively) and in σ_u from grain-to-grain could be included to treat statistical scatter.

Rain flow counting techniques (for which "real-time" algorithms are available)[20] will be used to express the local strains and stresses found by our deformation equations in terms of equivalent closed cycles. Five cumulative probability distributions describing these quantities are needed (see Fig. 4.1-2 for an example).

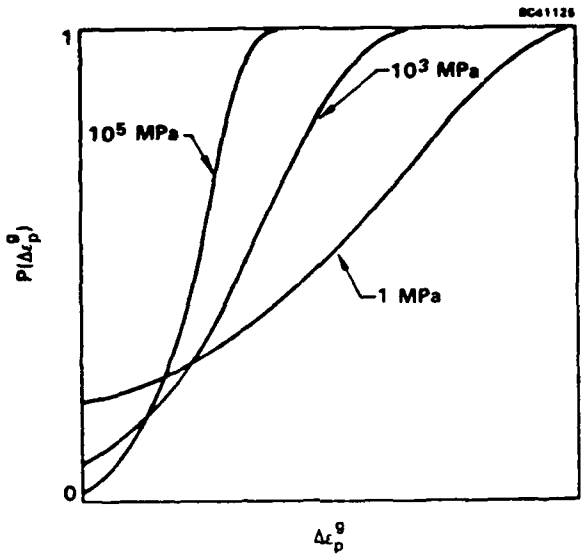

Fig. 4.1-2 Schematic cumulative distribution in $\Delta\varepsilon_p^g$ for a range in E_{pg} values resulting from a loading block.

$P(\Delta\varepsilon_p^g[E_{pg}])$; for the plastic strain range in the grain body

$P(\Delta\sigma_g[E_{pg}])$; for the stress range in the grain body

$P(\Delta^T\sigma_g[E_{pg}])$; for the positive stress range in the grain body

$P(\Delta^T\varepsilon_p^g[E_{pg}])$; for the positive plastic strain range in the grain body

$P(\Delta\varepsilon_p^m[E_{pg}])$; for the plastic strain range in the surface layer

Δ^T denotes the tensile portion of the cycle only, since crack growth only occurs on positive loading. The effects of load sequence, mean stress and stress amplitude are embedded in these distributions through their affect on the local stress-strain behavior.

4.1.1 Rain Flow Counting and the P Distributions

A typical output from the cycle-by-cycle strain calculations described in Sections 4.1.2 and 4.1.3 will be as in Fig. 4.1-3a. Rain flow analysis will be needed to reduce this spectra to equivalent closed cycles. The scheme is illustrated schematically in Fig. 4.1-3a and the result is tabulated in Fig. 4.1-3b giving a P distribution for one value of E_{pg}. In the following subsections, we discuss how the raw spectra on which this procedure will operate are obtained, and then how the block response functions are calculated.

4.1.2 The Stationary Grain Body Deformation Model [$\Delta\sigma_g$, and $\Delta\varepsilon_p^g$]

Assume σ_{max}^a and σ_{min}^a are the applied maximum and minimum stresses. There are five cases:

Case I: Loading from σ_{min}^a to σ_{max}^a, initial $\sigma_g < \sigma_u$; final load exceeds σ_u.

$$\Delta\sigma_g = \frac{[\sigma_{max}^a - \sigma_{min}^a - \sigma_u + \sigma_g]}{E_{pg} + \alpha_g E_e} \sigma_u - \sigma_g \qquad (4.1\text{-}1)$$

$$\Delta\varepsilon_p^g = \frac{[\sigma_{max}^a - \sigma_{min}^a - \sigma_u + \sigma_g]}{E_{pg} + \alpha_g E_e} \qquad (4.1\text{-}2)$$

where E_e is the bulk elastic modulus.

Case II: Loading from σ_{min}^a to σ_{max}^a with initial $\sigma_g > \sigma_u$

$$\Delta\sigma_g = \frac{[\sigma_{max}^a - \sigma_{min}^a]E_{pg}}{E_{pg} + \alpha_g E_e} \qquad (4.1\text{-}3)$$

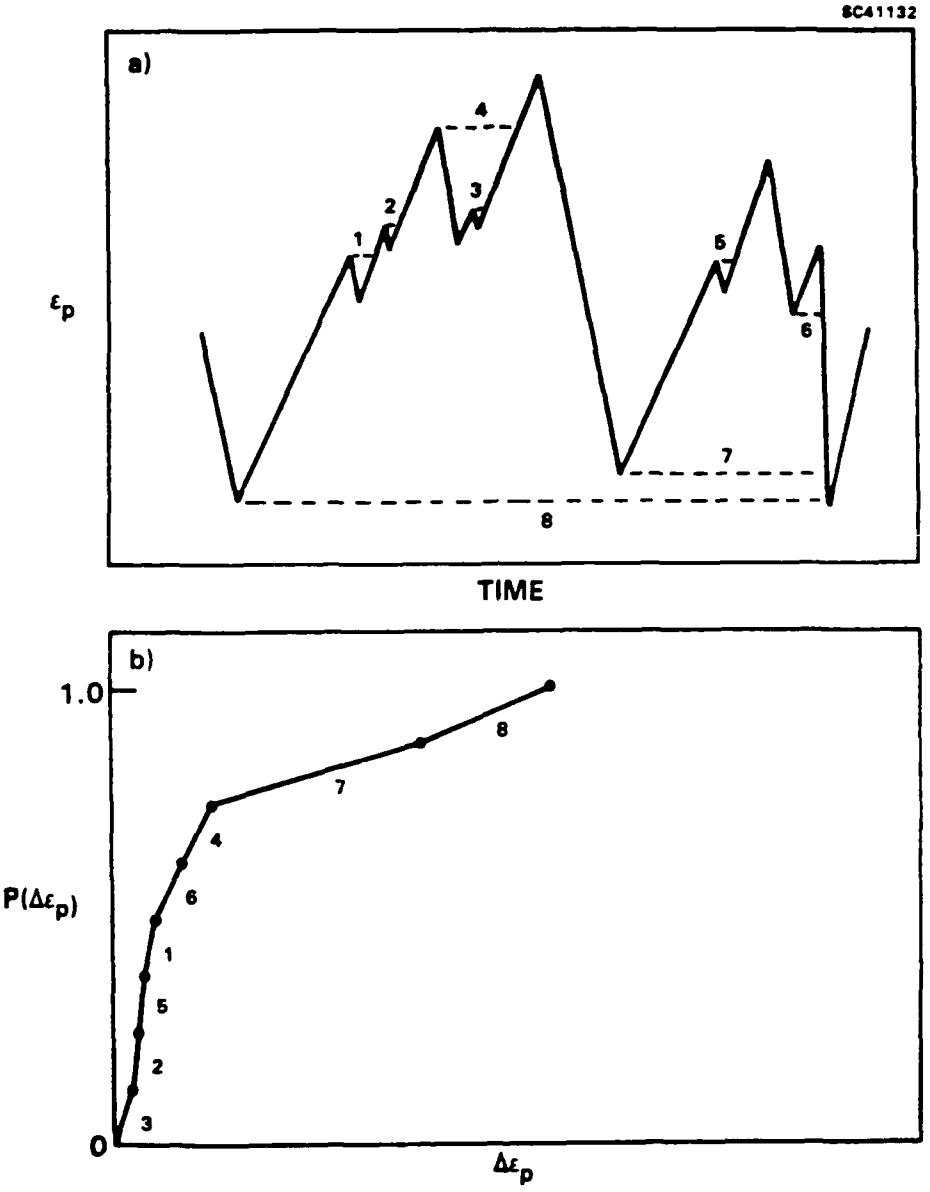

Fig. 4.1-3 Rain flow analysis procedures of local plastic strain on stress spectrum. (a) Raw spectra and rain flow lines (dashes); and (b) cumulative spectra distribution.

$$\Delta\varepsilon_p^g = \frac{[\sigma^a_{max} - \sigma^a_{min}]}{E_{pg} + \alpha_g E_e} \tag{4.1-4}$$

Case III: Always elastic.

$$\Delta\sigma_g = \Delta\sigma^a \tag{4.1-5}$$

$$\Delta\varepsilon_p^g = 0 \tag{4.1-6}$$

Case IV: Unloading from σ^a_{max} to σ^a_{min} with initial $\sigma_g > -\sigma_u$, final load less than $-\sigma_u$.

$$\Delta\sigma_g = \frac{[\sigma^a_{min} + \sigma^a_{max} + \sigma_u + \sigma_g]}{E_{pg} + \alpha_g E_e} - [\sigma_u + \sigma_g] \tag{4.1-7}$$

$$\Delta\varepsilon_p^g = \frac{[\sigma^a_{min} + \sigma_{max} + \sigma_u + \sigma_g]}{E_{pg} + \sigma_g E_e} \tag{4.1-8}$$

Case V: Unloading from σ^a_{max} to σ^a_{min} with $\sigma_g < -\sigma_u$

$$\Delta\sigma_g = \frac{[\sigma^a_{min} - \sigma^a_{max}]E_{pg}}{E_{pg} + \alpha_g E_e} \tag{4.1-9}$$

$$\Delta\varepsilon_p^g = \frac{[\sigma^a_{min} - \sigma^a_{max}]}{E_{pg} + \alpha_g E_e} \tag{4.1-10}$$

4.1.3 Kinematic Matrix Layer Deformation Model $[\Delta\varepsilon_p^m]$

Maximum σ_g^{max} and minimum σ_g^{min} values of σ_g taken from Sect. 4.1.2 are used to find $\Delta\varepsilon_p^m$. There are three cases. Separate values for the upper $\sigma_{\ell 1}$ and lower $\sigma_{\ell 2}$ flow stress of the layer must be calculated as these will change cycle-by-cycle

because the flow locus is kinematic. The local stress in the matrix layer, σ_m, will also change from the local stress in the grain body, σ_g.

Case I: Loading from σ_g^{min} to σ_g^{max} exceeding the prior $\sigma_{\ell 1}$.

$$\Delta\varepsilon_p^m = \frac{[\sigma_g^{max} - \sigma_g^{min} + \sigma_{\ell 1} - \sigma_m]}{E_{pm} + \alpha_m E_e} \tag{4.1-11}$$

$$\Delta\sigma_{\ell 1} = \Delta\sigma_{\ell 2} = E_{pm}\Delta\varepsilon_p^m \tag{4.1-12}$$

$$\Delta\sigma_m = E_{pm}\Delta\varepsilon_p^m + \sigma_{\ell 1} - \sigma_m \tag{4.1-13}$$

Case II: Always elastic.

$$\Delta\sigma_{\ell 1} = \Delta\sigma_{\ell 2} = 0 \tag{4.1-14}$$

$$\Delta\varepsilon_p^m = 0 \tag{4.1-15}$$

$$\Delta\sigma_m = \Delta\sigma_g \tag{4.1-16}$$

Case III: Unloading from σ_g^{max} to σ_g^{min}, falling below the prior $\sigma_{\ell 2}$.

$$\Delta\varepsilon_p^m = \frac{[\sigma_g^{min} - \sigma_g^{max} - \sigma_{\ell 2} + \sigma_m]}{E_{pm} + \alpha_m E_e} \tag{4.1-17}$$

$$\Delta\sigma_{\ell 1} = \Delta\sigma_{\ell 2} = E_{pm}\Delta\varepsilon_p^m \qquad (4.1\text{-}18)$$

$$\Delta\sigma_m = E_{pm}\Delta\varepsilon_p^m + \sigma_{\ell 2} - \sigma_m \qquad (4.1\text{-}19)$$

4.1.4 Slip Band Density, η

A crude estimate of η can be made from observations (Fig. 4.1-4) of the peak strains in grains vs the cyclic stress amplitude for fully reversed loading. Our observation are consistent with

$$\eta = \Delta\varepsilon_p^I . \qquad (4.1\text{-}20)$$

A proportionality constant needed in this expression has been embedded in E_o and E_o' in the equations used to calculate E_{pg} and ρ. Values at larger strains are taken from specimens first hardened at smaller amplitudes.

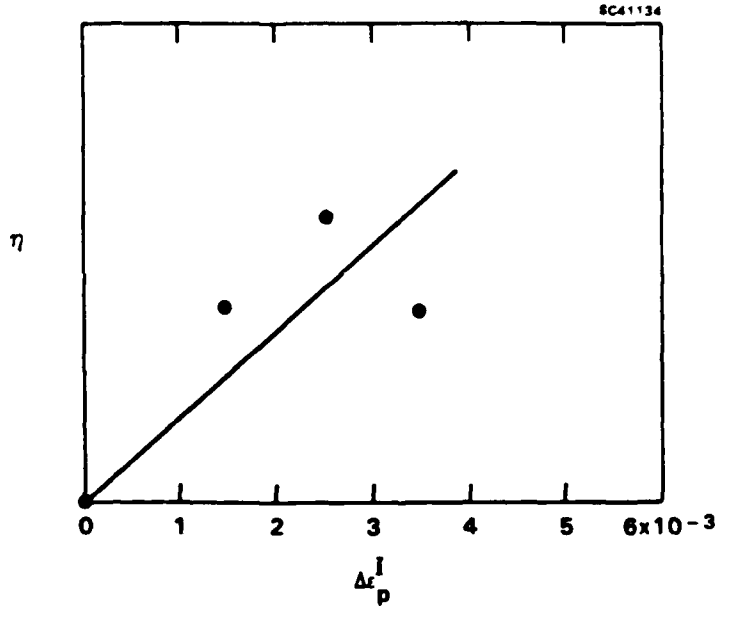

Fig. 4.1-4 Estimate of η made from peak residual strain amplitudes.

4.1.5 Incremental Hardening [ΔH]

Experiments indicate that at constant local cyclic stress, the cycles to harden a slip band can be expressed by Eq. (2.3-3). γ_3 and γ_4 are material parameters found by microscopic deformation observations. For spectrum loading, we propose a linear hardening rule, and obtain from Eq. (2.3-3) an incremental hardening of

$$\frac{1}{N} = 10^{-\gamma_3 10^{[\gamma_4(\Delta\sigma_g - 2\sigma_u)D]}} \qquad (4.1\text{-}21a)$$

for one cycle.

From whence,

$$\Delta H(E_{pg},D) = n \int_{2\sigma_u}^{\Delta\sigma_g} \frac{dP(\Delta\sigma_g)}{d\Delta\sigma_g} 10^{-\gamma_3 10^{[\gamma_4(\Delta\sigma_g - 2\sigma_u)]}} d\Delta\sigma_g \; . \; (4.1\text{-}21b)$$

An alternate approach, perhaps of use for treating microcracking of the slip bands themselves, might be to relate ΔH to the displacements in each band. These will be proportional to $\Delta\varepsilon_p^g/\rho$.

4.1.6 Increment in Slip Band Nucleation Damage (ΔI)

Apparently, a critical strain range must be exceeded in the surface layer for fatigue to activate slip at a potential nucleation site. Furthermore, these critical values of $\Delta\varepsilon_p^I$ vary from site to site. Our phenomological model which relates $\Delta\varepsilon_p^m$ at the site of activation $\Delta\varepsilon_p^I$ to the cycles to nucleate a band at constant amplitude is given in Fig. 2.3-2 and has been calibrated (γ_1, γ_2) by microscopic deformation data for Al 2219-T851.

We assume for spectrum loading, a linear accumulation of damage, ζ, and deduce for one cycle that

$$\frac{1}{\zeta} = \frac{\Delta\varepsilon_p^m}{\Delta\varepsilon_p^I} 10^{\frac{\Delta\varepsilon_p^m - \gamma_1}{\gamma_2}} . \qquad (4.1\text{-}22)$$

Hence,

$$\Delta I(E_{pg}, \Delta\varepsilon_p^I) =$$

$$\zeta \int_0^{\Delta\varepsilon_p^m} \frac{dP(\Delta\varepsilon_p^m)}{d\Delta\varepsilon_p^m} \cdot \frac{\Delta\varepsilon_p^m}{\Delta\varepsilon_p^I} 10^{\frac{\Delta\varepsilon_p^m - \gamma_1}{\gamma_2}} d\Delta\varepsilon_p^m . \qquad (4.1\text{-}23)$$

4.1.7 Increment in Crack Length (Δa)

First, we truncate the σ_g and ε_p^g spectra to their positive values before the rain flow analysis is done. Thereafter, we have

$$P(\Delta^T\sigma_g) \text{ and } P(\Delta^T\varepsilon_p^g)$$

containing n_s and n_p cycles, where n_s is the number of cycles in the stress spectra and n_p is the number of cycles in the plastic strain spectra, respectively. Because some of the cycles are elastic,

$$n_s > n_p .$$

By manipulating a model for crack tip opening ($\Delta\delta$) by Tompkins,[16] we obtain a cycle-by-cycle expression for the elastic-plastic incremental extension of a crack of length a.

$$\Delta a = A(\Delta\delta)^{\gamma n} \qquad (4.1\text{-}24)$$

where

$$\Delta\delta = a\left[\frac{(1.1)^2\Delta^T\sigma_g}{2E_e} + 0.4\pi\Delta^T\varepsilon_p^g\right]\Delta^T\sigma_g \ , \qquad (4.1\text{-}25)$$

from adaption of Tomkins equation.[16] Parameters A and γ can be determined by calibration from initiation lifetime data.

Since $\Delta^T\varepsilon_p^g$ is monotonically related to $\Delta^T\sigma_g$, we can perform a renormalization to allow Eq. (4.1-25) to be integrated over a loading block, without relying on a cycle-by-cycle tracking of the relationship of the local stresses and strains. The complexity to be cared for is that some of the cycles are entirely elastic.

For stresses less than $\Delta^{T'}\sigma_g$ defined by solving

$$\frac{n_s - n_p}{n_s} = P(\Delta^{T'}\sigma_g) \qquad (4.1\text{-}26)$$

there is no plastic strain.

For larger stresses, the equivalent $\Delta'\varepsilon_p^g$ is found by forcing a mapping of the stress range $\Delta'\sigma_g - \Delta\sigma_g$ to the strain range $0 - \Delta\varepsilon_p^g$. We have

$$\frac{n_s}{n_p}\left[P(\Delta^T\sigma_g) - P(\Delta^{T'}\sigma_g)\right] = P[\Delta^{T'}\varepsilon_p^g], \qquad (4.1\text{-}27)$$

and

$$\Delta^{T'}\varepsilon_p^g = P^{-1}\left[\frac{n_s}{p}\left(P(\Delta^T\sigma_g) - P(\Delta^{T'}\Delta\sigma_g)\right)\right] . \qquad (4.1\text{-}28)$$

Hence, the incremental change in crack length equals the sum of the elastic and plastic growth terms.

$$\Delta a = (n_s - n_p)A \int_0^{\Delta^T\sigma_g} \frac{dP(\Delta^T\sigma_g)}{d\Delta^T\sigma_g} \left[\frac{a(1.1)^2(\Delta^T\sigma_g)^{2\gamma}}{2E_e}\right] d\Delta^T\sigma_g$$

$$+ n_p A \int_{\Delta^T\sigma_g}^{\Delta^T\sigma_g} \frac{dP(\Delta^T\sigma_g)}{d\Delta^T\sigma_g} [a(\Delta^T\sigma_g)^2]^{\gamma} \left[\frac{(1.1)^2\Delta^T\sigma_g}{2E_e} + 0.4\pi\Delta^T\,{}'\varepsilon_p^g\right]^{\gamma} d\Delta^T\sigma_g \qquad (4.1\text{-}29)$$

4.2 The Intermediate Functions

The mathematical definitions of these functions are as follows [subscripts m and m-1 denote block numbers].

The grain size at which crack initiation occurs is calculated from

$$D = \sqrt{E_o(E_o' - E_{pg})(E_{pg}E_o'[\frac{\rho(D)}{D}]_{m-1})}^{-1} . \qquad (4.2\text{-}1)$$

which is written by solving Eq. 3.2-1a for D. The quantity $\rho(D)/D$ is independent of grain size and calculated in 4.4. Because of hardening, D is not always the largest grain size.

$$\Delta I(D, \Delta\varepsilon_p^I)_m = \Delta I(E_{pg_{m-1}}, \Delta\varepsilon_p^I) \text{ vs } D. \qquad (4.2\text{-}2)$$

$$I(D,\Delta\varepsilon_p^I)_m = I(D, \Delta\varepsilon_p^I)_{m-1} + \Delta I(D, \Delta\varepsilon_p^I)_m . \qquad (4.2\text{-}3)$$

$\Delta\varepsilon_p^{I_{max}}(D)_m$ is the solution to

$$I(D, \Delta\varepsilon_p^{I_{max}}(D))_m = 1 \ . \qquad (4.2\text{-}4)$$

$$\Delta H(D)_m = \Delta H(E_{pg_{m-1}}) \text{ vs } D. \qquad (4.2\text{-}5)$$

$$\Delta a(D)_m = \Delta a(E_{pg_{m-1}}, a) \text{ vs } D. \qquad (4.2\text{-}6)$$

$$a(D)_m = a(D)_{m-1} + \Delta a(D) \qquad (4.2\text{-}7)$$

at $m = 0$, $a = a_o$. A good value for a_o would be 20 μm for the Al 2219-T851 alloy used in our study. Initiation requires $a(D) = a_c$, where a_c is the critical initiation crack length which is equal to the grain depth.

4.3 The Cumulative Functions

These are:

$$H(D,m) = (\Delta H(D) + H(D, m-1)) \text{ vs } m \qquad (4.3\text{-}1)$$

$$\Delta\varepsilon_p^{I_{max}}(D, m) = \Delta\varepsilon_{p_m}^{I_{max}}(D) \text{ vs } m \ . \qquad (4.3\text{-}2)$$

4.4 Local Mechanical Properties

All bands initiated before m* blocks where

$$H(D, m) - H(D, m^*) = 1 \qquad (4.4\text{-}1)$$

have ceased to slip. Wherefore

$$\Delta\varepsilon_p^{I_{min}}(D) = \Delta\varepsilon_p^{I_{max}}(D, m^*) \; . \tag{4.4-2}$$

$\Delta\varepsilon_p^{I_{min}}(D)$ and $\Delta\varepsilon_p^{I_{max}}(D)$ allow $E_{pg}(D)$ and $\rho(D)$ to be found. $E_{pg}(D)$ is given by Eq. (3.2-6) and

$$\frac{\rho(D)}{D} = \int_{\Delta\varepsilon_p^{I_{min}}}^{\Delta\varepsilon_p^{I_{max}}} n(\Delta\varepsilon_p^I)\, d\Delta\varepsilon_p^I \; . \tag{4.4-3}$$

4.5 Initiation Lifetime

In its present form, the model just described is automatically calibrated for mean and sequence effects (for Al 2219-T851) by the microscopic deformation assessments. While all of the lifetime behavior could be handled this way, it is probably best to couple some of the model calibration to actual fatigue data. The simplest way to do this is to exercise the model for constant and fully reversed stress amplitude and for several values of γ (in Eq. (4.1-24)) in the range of 1-2 (reasonable theoretical estimates).

A comparison of predicted and experimentally determined initiation lifetimes would then be used to select the best values for A and γ. Thereafter, for any spectra applied to that alloy, A and γ used in lifetime calculation would remain the same.

The model will predict $a(D)$. This actually presupposes that there will be at least one surface grain of size D present in the stressed area, containing a constituent particle near the maximum size. Hence, $a(D) = a_c$ gives the cycles to initiation. If a large surface area is stressed, this will always be the case. But, as schematically illustrated in Fig. 4.5-1, if the stressed area is small the forecast from this model will be conservative, simply because the sites most vulnerable to initiation will not often be

present. In this case, a statistical calculation of the most probable initiation lifetime could be made and would require knowledge of the distribution in surface grain sizes (Fig. 4.5-2) and the stressed surface area. For completeness, the model must include stochastic variations in α_s, α_g, and σ_U, as mentioned earlier.

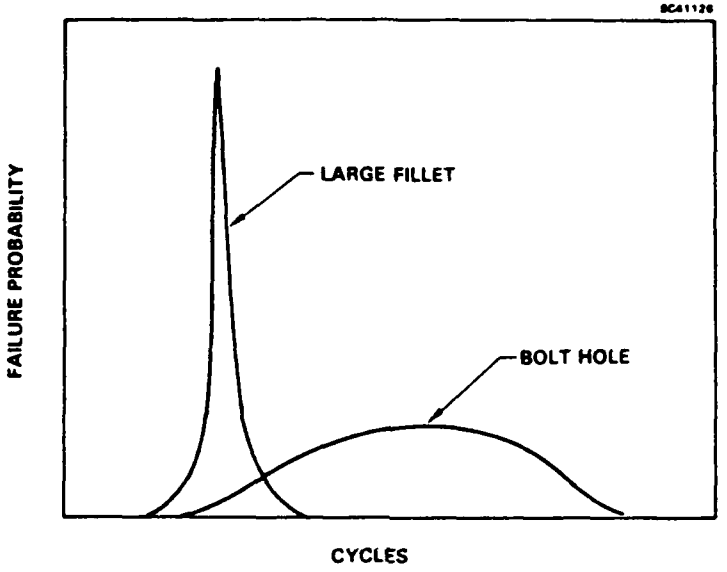

Fig. 4.5-1 Effect of surface area on initiation lifetime.

4.6 Step-by-Step Instructions for Modeling Initiation Lifetime in Al 2219-T851

4.6.1 The Cycle-by-Cycle Calculations

The purpose of the cycle-by-cycle analysis is to determine the local damage rate (over one loading block) due both to stress and plastic strain ranges for a grain of arbitrary size and mechanical properties. This calculation needs to be done for just one block, and allows us to determine the incremental change in mechanical properties, in hidden damage condition (degree of accumulative hardening of active bands, and predamage leading to new bands), and in crack extension.

1. Choose from the flight spectra a repetitive load block. (This will look like Fig. 4.1-3a, but for the applied stress rather than local stress.)

2. Decode this into a sequence of minimum and maximum stresses
$\sigma^a_{1min}, \sigma^a_{1max}, \sigma^a_{2min}, \sigma^a_{2max}, \cdots\cdots \sigma^a_{nmin}, \sigma^a_{nmax}$.

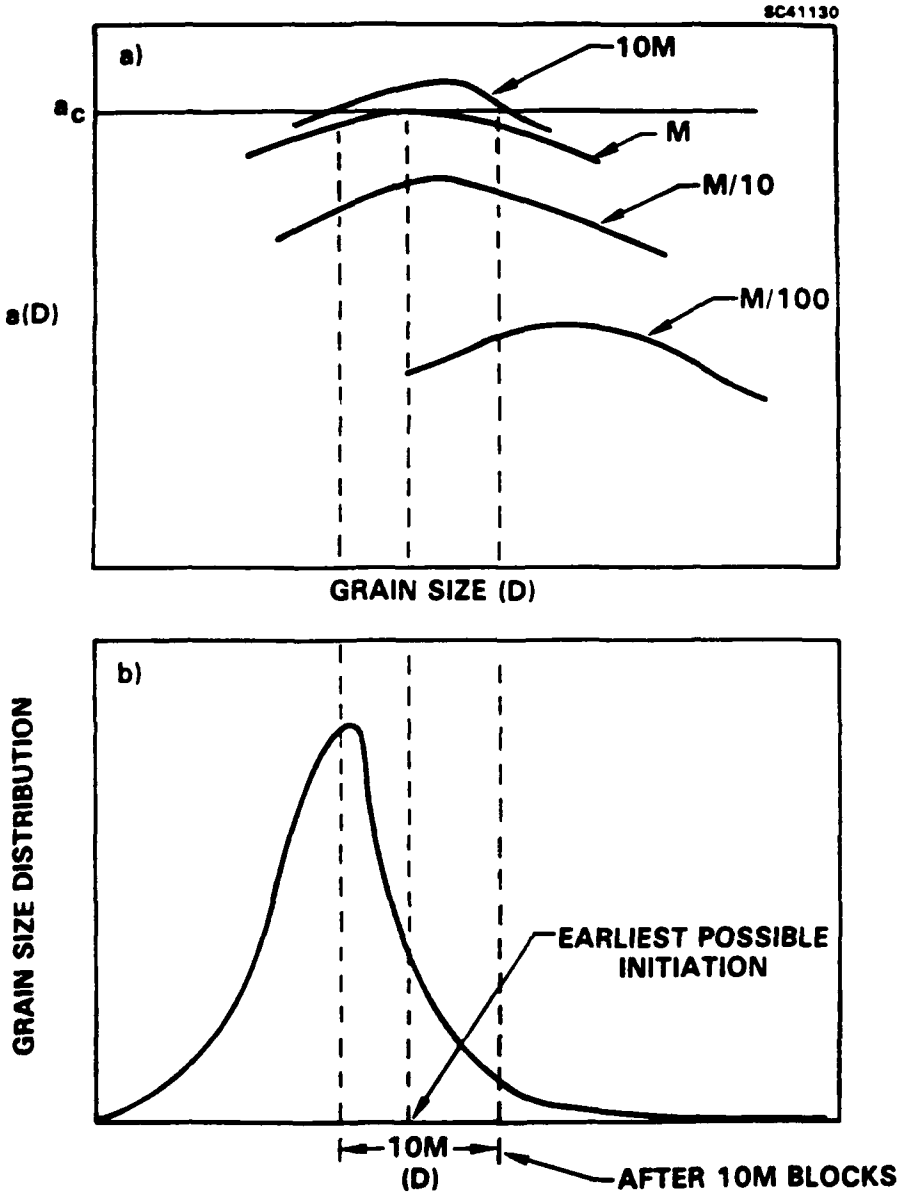

Fig. 4.5-2 (a) Evolution of the a(D) functions with cycles; and (b) resulting probability of initiation vs grain size.

3. For each half-cycle, determine the local stress/strains.

3a. Begin in the grain body with $\alpha_g = 0.75$, $\sigma_U = 140$ MPa, $E_o' = 100{,}000$ MPa, $\sigma_g = 0$, $\varepsilon_p^g = 0$.

3b. Calculate $\Delta\sigma_g$, $\Delta\varepsilon_p^g$, $\sigma_g = \sigma_g + \Delta\sigma_g$ for each half-cycle using Eqs. (4.1-1) to (4.1-10). This also defines a sequence σ_g^{min}, σ_g^{max} ... $\sigma_{g_n}^{min}$, $\sigma_{g_n}^{max}$.

3c. Consider the surface layer with $\alpha_s = 0.96$, $E_{pg} = 40{,}000$ MPa, $\sigma_\ell = 70$ MPa.

3d. Use the σ_g^{min}, σ_g^{max} sequence from 3b to find $\Delta\varepsilon_p^m$ half-cycle-by-half-cycle using Eqs. (4.1-11) to (4.1-19). For each half-cycle, also find $\sigma_{\ell 1}$, $\sigma_{\ell 2}$, σ_m^{min} and σ_m^{max} for use in the calculation on the next half-cycle. This will give sets of results which are displayed similar to the results in Fig. 4.1-3a. Both stress and strain range results must be compiled and this must be done for a selected set of possible values of E_{pg} in the grain's main body.

3e. Apply "real-time" rain flow algorithm to reduce $\Delta\sigma_g$, $\Delta\varepsilon_p^g$, $\Delta\varepsilon_p^m$, to equivalent fully reversed spectra. Truncate ε_p^g and σ_g to their positive values and apply rain flow to convert these positive going equivalents as well.

3f. At the completion of the block, arrange the elements of each of the five spectra in ascending amplitude and define the P distribution function and the intra-block cycle number for each, as the example in Fig. 4.1-3b.

3g. Repeat 3b-3f for new values of E_{pg}. It is likely that results for values of 10^5, 10^4, 10^3, 10^2, 10 and 1 MPa will suffice.

4. Use the P's to find ΔH, ΔI and Δa in terms of E_{pg} using Eqs. (4.1-21), (4.1-23) and (4.1-29).

4.6.2 The Block-by-Block Calculations

The block-by-block calculations deal with the progressive evolution of the the damage state space, and are supported by the property evolution results of the cycle-by-cycle analysis. The spectra response is embedded in the cycle-by-cycle analysis. This is just like a simpler conventional summation of cumulative damage (i.e., 1/n-type damage) except that the grain size, band densities, band hardening state, and predamage to form band states make the calculation multidimensional.

5. Begin with the first block. Set $a = a_o$, $E_o' = 100{,}000$ MPa.

5a. Use Eq. (4.2-2) to redefine ΔI in terms of grain size D. [On the first pass, $\Delta I(E_{pg}, \Delta\varepsilon_g^I)$ is independent of grain size.]

5b. Find $I(D, \Delta\varepsilon_p^I)$ and solve Eq. (4.2-4) for $\Delta\varepsilon_p^{I_{max}}$. For each grain size, this generates results as in Fig. 4.6-1, defining what fraction of potentially viable sites for band formation have produced bands.

5c. Likewise, find $\Delta H(D)$, $\Delta a(D)$ and $a(D)$ using Eqs. (4.2-4) through (4.2-7).

5d. Compare $a(D)$ to a_c to test for initiation.

5e. Find the cumulative functions H and $\Delta\varepsilon_p^{I_{max}}(D)$ [Eqs. (4.3-1) and (4.3-2)], and use these and Eqs. (4.4-1) and (4.4-2) to find $\Delta\varepsilon_p^{I_{min}}(D)$. See Fig. 4.6-2 for the construction used to find $\Delta\varepsilon_p^{I_{min}}$ for one grain size.

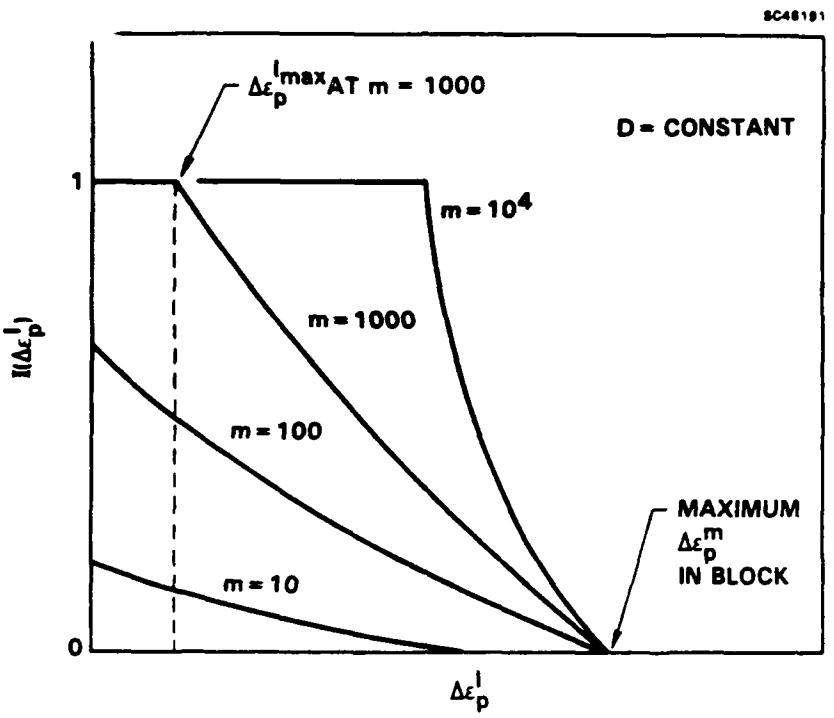

Fig. 4.6-1 Schematic illustration of $I(\Delta\varepsilon_p^I)$ for one value of D vs block number (m).

5f. Calculate E_{pg} and $\rho(D)/D$ [Eqs. (3.2-6) and (4.4-3)] and return to 5a to do the next block.

4.7 Model Calibration

The bulk of the material coefficients needed to calibrate this model have been defined by microscopic deformation observations for Al 2219-T851. Now that these elements have been identified, only a few weeks laboratory work would be required to obtain the calibration values for a new alloy. This would be accomplished by producing a sequence of measurable strains by fatigue (e.g., Ref. 5) from which the local stresses, state of constraint, and hence local flow stresses and strain hardening coefficient can be deduced. Growth parameters γ, A and a_o must be selected by comparison of the model predictions to measured initiation lifetimes for fully reversed loading before the spectrum loading calculations can be done. Likewise, E_o should be determined by a comparison of E_{pg} to experimentally determined values vs cycles at fixed amplitude using data such as in Section 2.1.

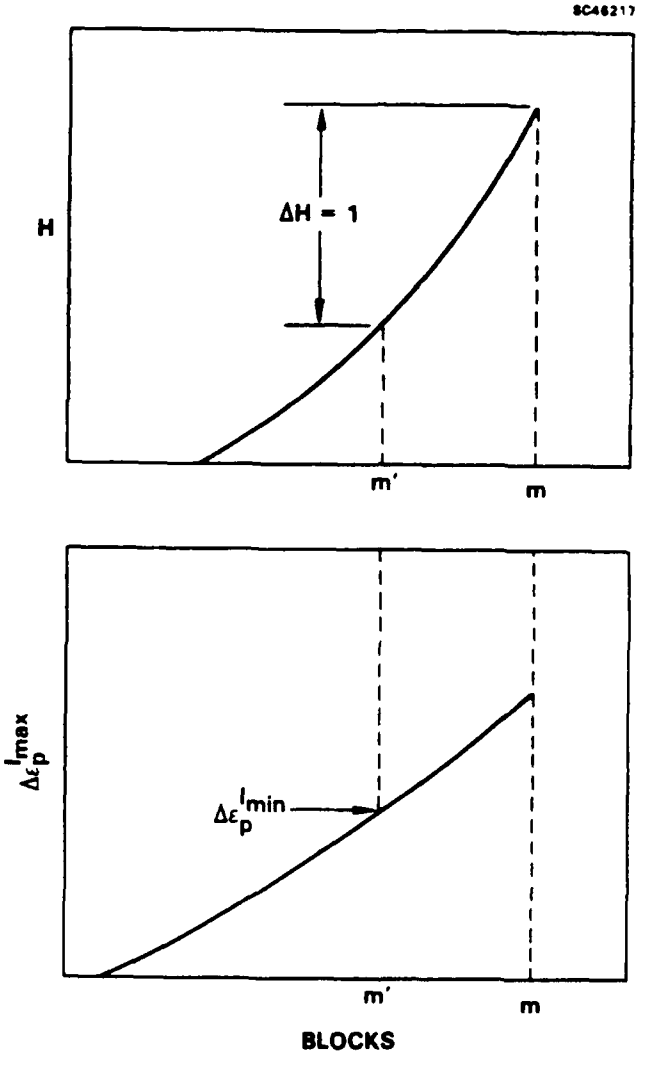

Fig. 4.6-2 Schematic illustration of procedure used to find the range $\Delta\varepsilon_p^{l_{min}}$ to $\Delta\varepsilon_p^{l_{max}}$ for which slip bands have both initiated and have not yet hardened. This defines (with η) the total number of active slip bands at block m in a grain of size D.

5.0 DISCUSSION

Mean stresses might affect a model material such as we have just described in several ways by:

1. Altering the local plastic strain ranges.
2. Changing the relationships of plastic strain to the response functions ΔH, ΔI and Δa. The first avenue is directly embedded in our half-cycle by half-cycle calculation of the local deformations. We have also proposed a truncation of $\Delta\epsilon_p^g$ prior to calculating Δa in an attempt to care for a mode I nature of the microcrack growth. Our experiments are insufficient to tell if ΔH and Δa respond to mean stress in addition to the local plasticity. However, investigators working along the same line with bulk low cycle fatigue behavior have concluded that this kind of mean effect is small, if it is present at all.

Effects of load sequence in our model will appear through

1. Their impact on the local plastic strains.
2. Because of an interaction with the hardening state H.

The extension of initiation lifetime of samples coaxed by low amplitude loading is directly attributable to the accelerated hardening of large compared to small grains in the alloy surface.[9] While a conservative lifetime prediction (and simpler numerical analysis) might result if hardening is omitted from the model, it is our surmise that an important potential impact of load sequence would also be lost from the predictions.

To what kinds of materials and loading situations would our model best apply? First, the deformation should be quasi-elastic in the bulk with strains less than 10^{-3}, for most of the load sequence. We hope, but it remains to be demonstrated, that occasional plastic overloads will not compromise our predictions, as long as the percentage of lifetime lost in the extremes is small. Second, the plasticity should be localized and,

hence, constrained. This might, for instance, happen in large grains in high strength structural alloys. It might also happen in soft spots that occur in some superalloys and titanium alloys. Structural aluminum alloys in a T6 or T8 heat treatment condition, for instance, should be representable. A large grained superalloy like WASPALOY and certain α-β titanium alloys are also candidates. Also, a fine-grained material such as IN100, "if it has soft spots", is a potential candidate, although the slip band portion of the model will probably need to be reworked for this material. If the alloy is cyclically stable or cyclically hardens, is employed below its bulk yield strength, and if it displays fatigue-induced changes in surface residual stress, indicative of localized flow, it is a candidate for this analysis.

What about possible alterations to the slip band nucleation model? Is it likely that the shallow surface layer of nucleation sites inferred for Al 2219-T851 is ubiqutious? Probably not. Our surmise is the confinement of band nucleation to a surface layer occurs only in coarse precipitation hardened alloys such as the overaged 2219. Yet to be established by experiment is the prospect that, in alloys where the hardening phase is more easily cut by dislocations, the nucleation sites for slip bands lie more deeply below the surface. In the limit that band nucleation can occur within the entire grain volume, our model requires a few mild alterations, which will actually simplify the numerical calculations.

1. The "surface layer" will become the grain volume with an appropriate α ($\approx$ 0.75 for pancake-shaped grains, and $\approx$ 0.4 for equiaxed grains).
2. ΔI will be calculated for the grain volume using the "kinematic model".
3. For equiaxed grains $E_{pg} \propto D^{-3}$, as the entire grain contributes to band initiation.
4. The local stress state must be calculated using a composite model of deformation as discussed in Section 2.2.

How might the crack initiation and lifetime controlling factors vary with alloy processing and with location in a structure. We believe that this approach will handle those alloys where soft spots in the surface matter. Materials such as cast iron, which contain initial flaws of grain size, will fail by crack growth at rates relatively insensitive

to local plasticity. But, the initiation lifetime of many of the high strength alloys clearly depend upon the micromechanics of local deformation. The effect of grain shape (and surface layers) on α (the proportionality constant between plastic strain and reaction stress) and hence on the relative importance of the local reaction stresses to plastic flow should largely determine how important load sequence and mean stresses will be to lifetime. If the reaction stresses are always small, because grains are deep and wide normal to the principal stress axis, the local and external loads will be nearly equal and sequence should be less important. Of course, the amplitude content of the spectra and its consequence to ΔH and ΔI will always matter. Reaction stresses will normally increase lifetime by lowering the plastic strain range. So, for identical spectra, local loading of a rolled plate in the transverse direction with an exposed transverse surface will likely accelerate initiation because of the very low α values of the pancake-shaped grains for that loading orientation.

Finally, what might alloy microstructure do to the crack initiation criterion and, hence, to the model we have described? Constituent particles common to structural aluminums will, if sufficiently large, nucleate cracks which progress to the grain boundary. If the alloy is overaged, the growth is more likely to be in Mode I and given by our model exactly as it is described. In this case, the largest typical particle depth would be appropriate to use as the starting crack size. If the surface area under stress is very small, a treatment of the statistical effects of particle size might be appropriate. If the aluminum alloy is in a peak hardness heat treatment, crystallographic growth from the initiation site is more likely. $\Delta\varepsilon_p^g$ should not be truncated before Δa is calculated if this is the case because the shear bands can slip in compression as well as in tension. Growth to the boundary of a crystallographic crack is likely to be mixed mode and respond to the local compressive as well as to the local tensile stress. In "clean" alloys having only very small particles, nucleation and growth of cracks in the slip bands themselves is likely. Then, we suspect that a microcrack growth analysis based on the quantity $\Delta\varepsilon_p^g/\rho$ might be most appropriate, as this is proportional to the strain in each individual band.

Still unresolved is how to handle those alloys in which grain boundary cracks are the fatal precursors. In Al 2219-T851, isolated boundary cracks form before the surface softens, apparently in response to the microscopic plasticity of the surface

layer. These cracks are very shallow (a few microns) and have not been found to propagate to failure. But, the mechanism which controls this behavior remains to be identified.

6.0 SUMMARY

In many structural alloys, crack initiation takes place at the surface in sites locally softened by fatigue. These areas behave just as material at the root of a notch when exposed to stresses exceeding yield. The plastic flow is constrained by the elastic member surrounding the notch, limiting the deformation and creating reaction stresses. These can cause stresses at the notch root to differ substantially from the externally applied stresses. Load sequence and mean stress then alter lifetime because the reaction stress modifies the coupling between load sequence and local plastic strain range.

For individual softened grains in an alloy, this picture is further complicated by the progressive change in strain softening/hardening behavior of each grain at rates dependent on grain size. In Al 2219-T851, one result is that cracking is focused in large grains at high cyclic stresses, and in somewhat smaller (although still larger than the mean size) grains at lifetimes close to the fatigue limit.

While we have a reasonable insight into the deformation constraints, there are clearly some loose ends in our overall understanding. In particular, the critical experiments to unequivocally demonstrate the presence of a thin surface layer of slip band nucleation in Al 2219-T851 remain to be done. Of more importance is the fact that the mechanics of the property evolution in single grains is largely understood only phenomenologically. The science which might allow one to make modifications in the model of property evolution to recognize failing cases, etc., remains to be done.

Nature is complex; but aircraft design must go on. Consequently, we have taken what we have learned about local surface deformation and the resulting cracking and embedded this in an initiation lifetime model. Our hope is that when this is calibrated using a minimum of test data, the resulting predictive power will be superior to more conventional empirical damage models. One reason for this hope is that our focus has been on understanding the underlying deformation which most assuredly controls initiation. Our understanding of the interplay between creation and hardening of slip bands as molded by the deformation constraints is also fairly comprehensive.

Just as with contemporary models, we propose the use of rain flow counting to reduce the calculated local stress and plastic strain spectra to a collection of fully reversed cycles for a loading block. But, this must be done to three different spectra, namely, the local stress and strain in the grain body and plastic strain in the surface layer within each grain. Each spectra is determined by a simple half-cycle-by-half-cycle calculation of stresses and strains within a grain over the duration of the block. The representation of these results in terms of a range of possible plastic moduli during individual blocks give a set of response functions describing increments in damage involving slip band nucleation, slip band hardening and incremental microcrack growth for a loading block. These functions, then, can be applied in sequence to predict the initiation lifetime to formation of a grain-sized crack vs the local grain size.

Mathematical models of the local grain stiffness, and the constrained plastic strain range are stated, and a phenomenological description of the slip band nucleation and band hardening rates vs the local plastic strain range or stress range are stated. Data to allow these submodels to be calibrated for Al 2219-T851 are presented. The piece that is missing from this work is the numerical framework to generate the loading block response functions. The equations to assemble these functions are stated and algorithms to do a "real-time" rain flow processing of the local spectra are available. Only the numerical means to construct smooth functions which include local stiffness variables in the three response functions must be formulated to create a working model. Thus, all the essential model elements have been defined, but the computer code to implement the initiation lifetime calculation for an arbitrary spectra must still be written.

7.0 RECOMMENDATIONS

This model is ready to be encoded and tested with a comparison of predictions to actual initiation lifetime vs loading spectra. If the model performs reasonably, it should be formulated into a user-friendly design tool. The next steps are:

1. To find out how well the model works for several classes of structural materials. The important variables and considerations are:

   Grain size
   Grain aspect ratio
   Surface layer presence/absence
   Deformation mode (slip bands vs local Mode I cracking)
   Stress amplitude content
   Load sequence
   Mean stress
   Statistical (and notch) effects with an appropriate model refinement

2. To identify appropriate ways to calibrate the model by determination of responses to standard load spectra, in order to minimize the information needed in the local deformation behavior and grain size distribution.

3. To explore alternate mathematics to implement this model. We have described a quasi-sequential calculation of average lifetime. Other avenues possibly computationally more efficient are state space evolution and probabilistic formulations.

8.0 REFERENCES

1. H.O. Fuchs, D.V. Nelson, M.A. Burke and T.L. Toomay, "Shortcuts in Cumulative Damage Analysis," Fatigue Under Complex Loading: Analysis and Experiments, Vol. 6, R.M. Wetzel, ed., SAE, Warrendale, PA (1977), p. 145-162.

2. L. Tucker, S. Downing, L. Carrillo, "Accuracy of Simplified Fatigue Prediction Methods," Ibid, p. 137-144.

3. M.R. Mitchell, "Fundamentals of Modern Fatigue Analysis for Design," ASM Fatigue and Microstructures, 385-437 (1979).

4. W.L. Morris, B.N. Cox and M.R. James, Acta Metall. 35, 1055-1065 (1987).

5. B.N. Cox, W.L. Morris and M.R. James, Acta Metall. 35, 1289-1300 (1987).

6. W.L. Morris, M.R. James and B.N. Cox, "The Evolution of Local Mechanical Properties of Al 2219-T851 During Fatigue," Fatigue 87, ed. R.O. Ritchie and E.A. Starke, EMAS, 93-101 (1987).

7. M.R. James and W.L. Morris, "Load Sequence Effects on the Deformation of Isolated Microplastic Grains," Effects of Load and Thermal History on Mechanical Behavior, ed., P.K. Liaw and T. Nicholas, TMS-AIME, 147-152 (1987).

8. W.L. Morris, M.R. James and B.N. Cox, Mat. Sci. Eng. 94, 137-145 (1987).

9. M.R. James and W.L. Morris, Mat. Sci. Eng. 56, 63-71 (1982).

10. W.L. Morris, B.N. Cox and M.R. James, "Investigation into the Fatigue Crack Initiation Process in Metals," Final Tech. Report, Naval Air Development Center, Contract No. N62269-83-C-0267 (1985).

11. W.L. Morris, M.R. James and O. Buck, Met. Trans. 12A, 57-64 (1981).

12. W.L. Morris, Met. Trans. 11A, 1117-1123 (1980).

13. J. Lankford, D.L. Davidson and K.S. Chan, Met. Trans. 15A, 1579-1588 (1984).

14. R.A. Smith, Int. J. Fract. 13, 717-720 (1977).

15. K.J. Miller, Fat. Eng. Mat. Struct. 5, 223-232 (1982).

16. B. Tomkins, Met. Sci. 6, 408-417 (1980).

17. M.R. James and W.L. Morris, "The Effect of Microplastic Surface Deformation on the Growth of Small Cracks," Small Fatigue Cracks, R.O. Ritchie and J. Lankford, eds.,145-156 (1986).

18. J. Lankford, Fat. Eng. Mat. Struct. 5, 233-248 (1982).

19. J.M. Finney and A.D. Denton, "Cycle Counting and Reconstitution with Application to Aircraft Fatigue Data Analysis System Analysis," Proceedings of the International Conference on Fatigue Engineering Materials and Structures, University of Sheffield, September 1986.

20. D.G. Ford, "Range-Mean-Pair Exceedances in Stationary Gaussian Processes," ARL, IFIP paper, Aalboy, Den, May 6-8, 1987.

APPENDIX A

Appendix A was presented at the Fatigue 87 Conference in Charlottesville, VA, June, 1987.[6] The notation is essentially the same as through the main body of this report. The figures and references for this section are self-contained.

NADC-89044-60
FATIGUE 87

Rockwell International
Science Center
SC5470.FR

THE EVOLUTION OF LOCAL MECHANICAL PROPERTIES OF Al 2219-T851 DURING FATIGUE

W.L. Morris , M.R James' and B.N. Cox

Local strain amplitudes were measured in individual grains of an Al 2219-T851 alloy during fatigue. The alloy has a 360 MPa bulk cyclic yield strength, but its surface is microplastic at cyclic stresses greater than 70 MPa. With fatigue at ± 275 MPa, an upper flow stress of - 200 MPa develops in grains much larger than the mean size. Large residual stresses caused by constraint of the localized deformation severely limit the total strain at these softened sites. The use of a load reduction sequence to minimize these residual stresses during strain measurements, so as to obtain more accurate values for the local flow stresses, is discussed.

INTRODUCTION

Large local residual stresses are always present during inhomogeneous deformation (1,2). In fatigue-softened alloys, localized deformation is modified by residual stresses resulting from constraint of flow by the harder surroundings (3,4). Even on a smooth surface, deformation inhomogeneity at the grain level ensures the presence of these residuals, and hence a substantial difference between the local and externally applied stresses. A simple analysis has shown (3) that the residual stress in individual grains can easily be so large that portions of a grain can be in compression while the external stress is tensile. This complicates a simple determination of the local flow stress of individual grains in alloys.

In two recent papers (3,4), we used models of the deformation of a soft ellipsoid in an elastic matrix to calculate the flow stress and strain hardening characteristics of surface grains in Al 2219-T851. The models account for the local residual stress, allowing for the interpretation of strains measured in individual

Published in Fatigue 87, ed. R.O. Ritchie and E.A. Starke, EMAS, 93-101 (1987).

grains as a function of external stress. We find that fatigue of Al 2219-T851 at stresses below its bulk cyclic yield strength causes a reduction in the local 0.2% offset yield strength of the interiors of the grains, with preference for the largest surface grains. Grains 3-8 times larger than the 60 μm mean are the most affected and are also the eventual sites of crack initiation. Ultimately, the yield strength of these grains falls to half the bulk cyclic value, and well below the applied cyclic stress amplitude. However, the local strain amplitude typically remains less than 10^{-3} in these softened grains because the deformation is constrained by the nearly elastic surface.

These results seem in conflict with ample evidence that many alloys locally harden (5,6). Even in Al 2219-T851, Knoop indentation shows that fatigue hardens the interiors of individual grains, with the change being greatest in the largest grains (Fig. 1). Previous local strain measurements in this alloy have shown that, in large grains, the width of the local strain-external stress hysteresis loop at zero stress reaches a peak with fatigue and then decreases in amplitude, again suggestive of hardening (7).

In this paper, we demonstrate that the small local flow stresses deduced from strains measured within individual grains are not an artifact of our deformation analysis. While strain hardening parameters and deformation depth cannot be accurately obtained without a rigorous theoretical analysis, the local flow behavior can be found directly. A load reduction sequence is used to minimize the local residual stress, causing the external and local stresses to be nearly equal. This technique is used to characterize the evolution with fatigue of flow stresses and strain hardening at low plastic strain amplitudes in a 300 μm grain in Al 2219-T851. The apparent conflict between indentation and local strain measurements is not completely resolved, but the new local stress-strain data provide some clues to possible answers to this problem. We believe that the 10% strains encountered during indentation (8) can make this method a misleading probe of the highly constrained yielding which occurs in isolated softened grains, in which the maximum plastic strains are only 10^{-3} during typical fatigue experiments.

EXPERIMENTAL TECHNIQUES

The 360 MPa yield strength Al 2219-T851 had a 60 μm average grain size in the rolling plane measured at 45° to the rolling direction. The grains were pancake shaped, being nominally 20 μm deep. Tapered flexural specimens (9) of the alloy were carefully machined and polished to minimize initial residual surface stresses and then chemically etched to reveal the grain boun-

daries. Fatigue was in bending at nominally ± 275 MPa in dry nitrogen. The local strains reported were measured using a reference gauge placed within the center of grains and at least 25 μm from the nearest boundary by a micromanipulator, and with the aid of a loading jig in a scanning electron microscope (SEM), as described in Ref. 10. The reference gauge is a thin mica flake used as a convenient ruler and attached to the substrate electrostatically so that the surface can deform freely beneath it. It acts as a stable length, needed to compensate for the $\pm 5 \times 10^{-3}$ magnification instability of our SEM. Distortion and parallax errors from the ruler are smallest at zero load, where we made most of our measurements. For fully reversed loading, the width of the local strain-external stress hysteresis loop at zero load was found by comparing a micrograph taken after completing the compressive cycle to one taken after the next tensile cycle. The information needed to deduce flow stress, strain hardening and constitutive relationships was obtained by changing the loading sequence prior to the loop width measurement (4). We used a stereoscopic analysis of the micrographs to maximize the sensitivity of measurements of the surface displacements relative to the ruler. Since the displacements of nearly identical high contrast objects in each pair of micrographs were found, the accuracy was much better than the point-to-point resolution of the SEM. The displacement of any high contrast profile can easily be determined to a small fraction of the profile width. It is the image reproducibility which actually matters. The quality of our SEM images has been progressively improving over the past few years and we can now achieve about ± 15Å in-plane displacement sensitivity.

RESULTS

To determine how the flow stress of a grain's interior progressively changes during fatigue, we interrupted the constant amplitude cycling at intervals, and determined the local flow stress by measuring strains within the grain for a series of reduced cyclic loads. The local mechanical properties in Al 2219-T851 change slowly, so this measurement activity has no significant effect on the property evolution. The cyclic stress was dropped to a value σ and six cycles were applied to allow the local stress-strain hysteresis to reach equilibrium (4). Then the residual strain at zero external load was measured over a tensile loading cycle. The strain found at each σ is the width, W_o, of an external stress-local strain hysteresis loop at zero external load. W_o will always be smaller than the zero load width of a local stress-local strain loop because of local residual stress. As the measurement stress σ is decreased, W_o at equilibrium becomes progressively smaller. At the same time, the maximum local residual stress within the grain decreases because the maximum local plastic strain amplitude has decreased. For a

sufficiently small plastic strain amplitude, the difference between the external and local stresses at equilibrium will be small, and an accurate determination of the local flow stress can be made from W_o vs σ. An upper bound on the local residual stress magnitude is given by the product of the local plastic strain and the alloy modulus (3). For aluminum, the modulus is nearly independent of grain orientation, and the maximum plastic strain is rarely 5 times larger than W_o; so for W_o's smaller than 5×10^{-5}, the difference between external and local stress should be less than 20 MPa after equilibrium is reached. Only resolved shear stress variability due to grain orientation should remain.

High sensitivity measurements of W_o made early in fatigue show the surface is microplastic at stresses greater than 70 MPa (Fig. 2). In fact, the stress dependence of W_o for a very large (300 μm) and a smaller (120 μm) grain are essentially identical. We would expect to see more scatter in such results from resolved shear stress with more measurements but, clearly, the deformation in the essentially unfatigued alloy is short ranged in that it does not sense the grain boundaries.

With continued fatigue, a dramatic change in loop width occurs in just the largest grains. Figure 3 compares the behavior of a 300 μm grain after 100 and 250 cycles. Within the $\pm 1.5 \times 10^{-5}$ measurement sensitivity, there is little change in the lower flow stress (σ_ℓ, at $W_o = 1 \times 10^{-5}$) with fatigue. But, characteristic of large grains in the alloy is the appearance of an upper flow stress, σ_U, in this case seen clearly after 250 cycles. Below σ_U the grain has apparently strain hardened with fatigue (i.e., $dW_o/d\sigma$ has decreased); above σ_U, the grain has strain softened. We have shown the results in Fig. 3 on a logarithmic scale to clarify the data at small strains. When these and similar data at other fatigue increments are plotted linearly, trends in σ_ℓ and σ_U with fatigue are more accurately defined (Fig. 4a), and indirect information on the strain hardening behavior can also be obtained (Fig. 4b) by treating the strain as linear with σ above and below σ_U. A theoretical analysis of loop widths for such two-stage yielding is presented in Ref. 4.

We see from Fig. 4a that the local flow stresses are nearly constant in a 300 μm grain with perhaps a small fatigue induced decrease in σ_U. The important changes with fatigue are in $dW_o/d\sigma$. The quantity $dW_o/d\sigma$ is shown for the stationary yield surface approximation in Ref. 4 to be equal to $2(1-\alpha)/(2E_p + \alpha E_e)$; where α has a value less than 1 and is a proportionality between the local residual stress and the plastic strain determined by deformation depth, grain shape, and Poisson's ratio. E_p and E_e are plastic and elastic moduli. An increase in $dW_o/d\sigma$ means that either E_p or α has decreased. Typical values for α will be between 1 and 0.6, with very shallow deformation raising α. A full interpretation of the $dW_o/d\sigma$ results in Fig. 4b requires

additional W_o vs load sequence data so that α and E_p can be independently determined (see Ref. 4). However, if the depth of deformation within the grain is reasonably constant, the results mean that between 100 and 500 cycles E_p has increased below σ_u and has decreased above σ_u, i.e., the grain has strain hardened below σ_u and strain softened above σ_u. A more complete analysis, to be described later, suggests that the fall in $dW_o/d\sigma$ at 800 cycles and above σ_u is a consequence of a reduction in the depth of the deformation within the grain. The results shown at 500 cycles are for a different 300 μm grain, so considerably more data are needed to completely sort out the fatigue-induced evolution of local strain hardening and deformation depth.

DISCUSSION

It is simplistic to think of the fatigue-induced changes in local surface deformation of Al 2219 as reflecting traditional hardening or softening. The changes are complex and partially hidden by the large residual stresses developed by constraint of the local deformation. Analysis in Ref. 4 shows that by 500 cycles σ_u is just below the conventional (0.2% offset strain) yield strength. The loop width measured at maximum cyclic stress is small because the deformation is constrained. Mughrabi's (11) concept of treating the flow of such a material as that of a composite of matrix and penetrating channels or slipbands seems relevant here. But unlike the case of Cu, it appears to us that the upper rather than the lower flow stress more likely corresponds to long-range dislocation motion. The argument for this is indirect. First, σ_u develops after fatigue. While PSB's are not optically visible in Al 2219-T851, banded slip has been found by high resolution strain field analysis in large grains after fatigue (3), suggestive of a connection to σ_u. Second, before there is substantial fatigue damage, the flow above σ_t is independent of grain size and, therefore, probably short range and in the matrix.

No substantial change in the flow characteristics of small grains has been found after 10^4 cycles at ± 275 MPa, while in 300 μm grains changes both above and below σ_u are apparent after a few hundred cycles. So, if there is strain hardening below σ_u in the matrix, it must have accompanied the formation of the long-range dislocation structure which deforms above σ_u, and cannot instead be the cause of the long-range structure. Otherwise, matrix strain hardening would take place over the entire surface early in the lifetime.

How might an indentation test perceive a composite grain in which the matrix had strain hardened, and in which banded slip had developed for which flow above σ_u up to strains of perhaps 10^{-3}

was nearly perfectly plastic? Clearly, on the basis of a lower 0.2% offset yield strength, fatigue has softened the larger grains, but there are several ways that indentation might sense hardening. The strains at the tip of a pyramidal indenter are relatively insensitive to indentation depth and are nearly 10^{-1} (8). Any mechanism which exposes the matrix to indentation and suppresses the contribution of flow from the bands will sense fatigue hardening. Possibilities for this include a saturation of the strain in the bands at the much higher strain of indentation, or the destruction of the long-range slip mode by the indentation. Naturally, we do not believe that softening is being universally misinterpreted as hardening. We have recently found unequivocal local cyclic hardening of an Al-4% Cu alloy with the same local strain measurement techniques. Our results simply call for care in the analysis of local mechanical properties.

We have known since the work reported in Refs. 3 and 4 that deformation in large (300 μm) grains in Al 2219-T851 eventually becomes nearly perfectly plastic during fatigue (i.e., $E_p \approx 0$). While it has been clear that reaching this state involved a dramatic drop in the local yield strength, it was not clear if the evolution of the local mechanical properties entailed a decrease in σ_u, a decrease in E_p, or changes in both these quantities. It now appears likely that, while both may be changing, the most important effect is on E_p.

SUMMARY

Strains measured in individual grains of Al 2219-T851 show a progressive evolution of the local mechanical properties. The entire surface is microplastic at fully reversed stresses greater than ± 70 MPa. Early in fatigue, the deformation strains are independent of grain size, suggesting that the flow resides in a matrix subject to short-range constraints. With continued fatigue, an upper flow stress σ_u becomes visible at ~ 200 MPa in grains substantially larger than the mean size. Below σ_u, the material apparently strain hardens, above σ_u it strain softens. The possibility that the development of σ_u coincides with the penetration of the matrix by slip bands is suggested.

Acknowledgements

This research was supported by NADC under Contract No. N62269-86-C-0261. Our thanks are expressed to R.V. Inman for taking the surface deformation micrographs.

REFERENCES

(1) Asaro, R.J., Acta Metall. 23, 1975, pp. 1255-1265.
(2) Margolin, H. Hazaveh, F., and Yaguchi, H., Scripta Met. 12, 1978, pp. 1141-1145.
(3) Morris, W.L., Cox, B.N., and James, M.R., "Microplastic Surface Deformation of Al 2219-T851," to be published in Acta Metall.
(4) Cox, B.N., Morris, W.L, and James, M.R., "Two-Stage Microplastic Surface Deformation in Al 2219-T851," to be published in Acta Metall.
(5) Thompson, A.W., Acta Metall. 23, 1975, pp. 1337-1342.
(6) Margolin, H., and Stanescu, M.S., Acta Metall. 23, 1975, pp. 1411-1418.
(7) James, M.R. and Morris, W.L., Mat. Sci. and Engrg. 56, 1982, pp. 63-71.
(8) Atkins, A.G. and Tabor, D., J. Mech. Phys. Solids 13, 1965, 149-164.
(9) Zurek, A.K., James, M.R., and Morris, W.L., Met. Trans. 14A, 1983, pp. 1697-1705.
(10) Morris, W.L., Inman, R.V., and James, M.R., J. Matl. Sci. 17, 1982, pp. 1413-1419.
(11) Mughrabi, H., Acta Metall. 31, 1983, pp. 1367-1379.

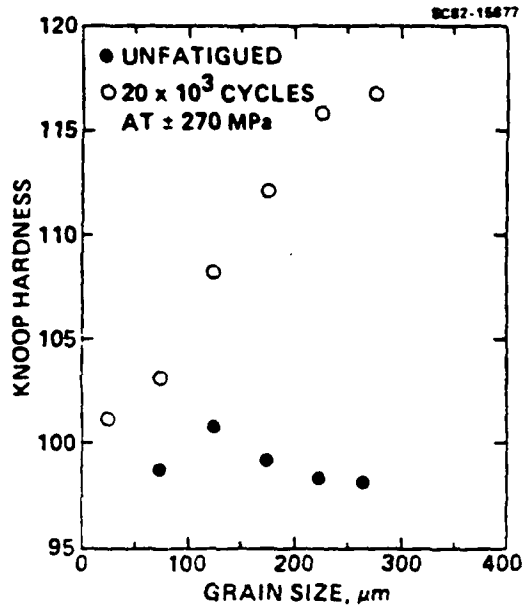

Figure 1 Knoop hardness of Al 2219-T851 vs the individual grain size in a single specimen shows apparent hardening after fatigue. Each datum is an average of approximately ten measurements.

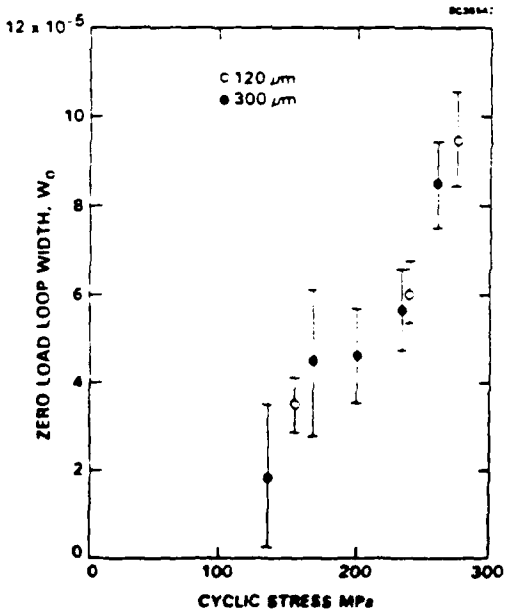

Figure 2 Comparison of loop widths measured at zero load vs cyclic stress amplitude for a 120 and a 300 μm grain. The data were obtained before a substantial fatigue induced change in deformation has occurred.

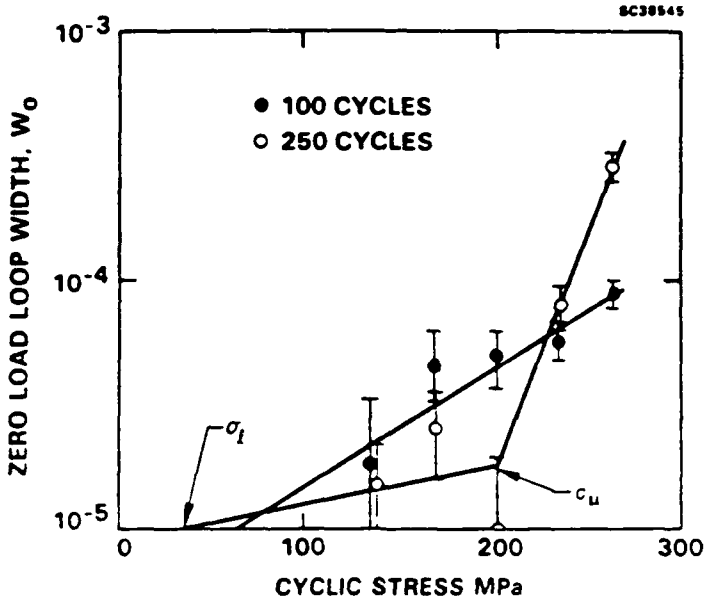

Figure 3 The progressive change in loop width in a 300 μm grain with fatigue.

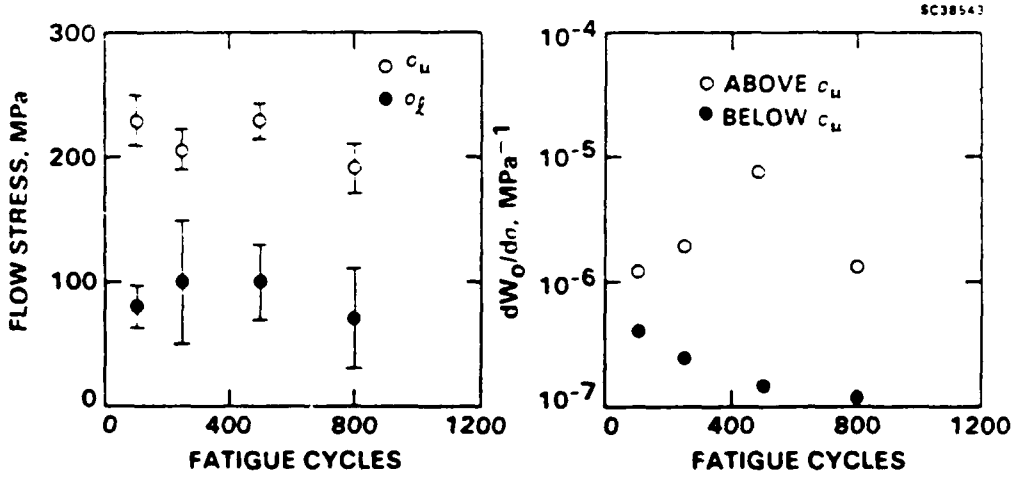

Figure 4 Trends in (a) σ_ℓ and σ_u; (b) $dW_o/d\sigma$ above and below σ_u for the 300 μm grain.

APPENDIX B

Appendix B was presented at the Spring 1987 meeting of the TMS-AIME in Denver, CO, in February, 1987.[7] The notation used is essentially the same as in the main body of this report. The figures and references in this section are self-contained.

NADC-89044-60

Rockwell International
Science Center
SC5470.FR

LOAD SEQUENCE EFFECTS ON THE DEFORMATION OF ISOLATED MICROPLASTIC GRAINS

M.R. James and W.L. Morris

Rockwell International Science Center
1049 Camino Dos Rios
Thousand Oaks, CA 91360

Abstract

Strains measured in individual large grains of Al 2219-T851 are used to deduce the local constitutive behavior that controls plastic flow under spectrum loads. A composite model for the deforming grain is most consistent with experiment. The material apparently contains two intermingled dislocation structures whose flow is controlled by different yield criteria. Special load sequences are used to determine the yield criterion best descriptive of each component, based on strains measured over 100 μm gauge lengths in individual grains.

Introduction

Even for "elastic" loading, the role of inhomogeneous localized plasticity in fatigue has been demonstrated repeatedly (1-3). Recent theories of inhomogeneous plasticity in tensile and cyclic loading principally consider large strains and show the importance to plastic flow of inhomogeneity in alloy microstructure (4,5) (e.g., granularity) and of local instabilities in deformation (6). When dislocation phenomena have been used to model the constitutive response of local elements in a material, it is often supposed that the underlying events of dislocation generation, saturation and recovery are sequential and conditioned on the local total strain range. However, for the small plastic strains common to most structural fatigue failures, the dislocation structures themselves tend to be inhomogeneous. Dislocation channels or bands penetrate a matrix of dislocation tangles, creating a microscopic composite (7-9). The local stress state in such subelements, their local mechanical properties and constitutive response may all differ, and each quasi-homogeneous material element will "remember" prior deformation and react to factors beyond total local strain and stress. A complex interaction between load sequence, local stress-strain response and rates of fatigue crack initiation can be anticipated for all such materials.

Recent studies of the deformation of individual large grains in an overaged aluminum alloy (10-14) suggest the importance of a "composite" dislocation structure in modeling the local strain - external stress response. The flow of each isolated microplastic grain is constrained by the nearly elastic surface, creating reaction stresses reminiscent of those at the root of a locally plastic notch. Procedures have been developed (10,11) to determine the mechanical properties of isolated plastic grains from strains measured over microscopic (< 100 μm) gauge lengths. The local internal stresses that might affect the measured property values are handled by load shedding, which either reduces the stresses (12), or allows the resulting plastic hysteresis to be analyzed (10,11). After fatigue of Al 2219-T851, marked hardening of the plastic flow is observed below a critical stress, above which there is simultaneous and dramatic strain softening (12). Does this softening herald the development of banded slip, seen only by high resolution strain field mapping (13) in 2219, or is it better explained by the saturation and recovery mechanism of a single subcomponent of the material, utilized by Estrin and Kubin (6) in modeling inhomogeneous plasticity?

To resolve this question we examine the local constitutive behavior of individual grains by studying their response to several load sequences. In particular, we determine what constitutive behavior, in terms of motion of the yield locus, must be assigned to each element of a two-component composite in order to achieve the observed stress-strain reaction to mean stress and tensile reloadings found experimentally.

Background

When Al 2219-T851 is loaded cyclically below its 360 MPa cyclic yield strength, the initial strains in a 300 μm grain found over a tensile increment are small, but discernible above the experimental measurement error, at stresses greater than 70 MPa (σ_L) (Fig. 1a). A few hundred cycles at ± 270 MPa changes the local properties of the grain, creating an upper flow stress (σ_U) near 200 MPa, strain hardening below σ_U, and softening above (Fig. 2a) (12). The technique used to measure strains over the 100 μm gauge lengths required for this study (see Refs. 10, 11, 15, 16) employs displacements measured between two points of zero external load in a loading sequence. The total strains calculated from the displacements reflect reactions to local plasticity (residual), rather than the elastic strains stemming from an external load. If the residual strains are less than $\sim 4 \times 10^{-5}$ the reaction stresses will typically be sufficiently small that data such as in Fig. 2a will depict the true local stress-strain response. If the residual strains are large, deformation models are needed to separate the elastic reaction strain and plastic strain components, in order to identify flow points and calculate strain hardening coefficients.

Deformation Models

Other studies on Al 2219-T851 (10,11) indicate that in the overaged state, local mechanical properties do not vary greatly across a grain so that an assumption of uniform plastic deformation is adequate for fully reversed loading. Two limiting cases of the flow surface locus have been examined for microplastic grains, namely: 1) a "stationary" surface (S) independent of prior load; and 2) a "kinematic" surface (K), which moves freely with the maximum stress excursion on the previous load reversal (11). With the S model, the grain has no memory of being deformed other than its instantaneous plastic strain and the resulting reaction to its constraint by the grain boundaries, while with the K model a maximum possible "back stress" is remembered in addition to plastic strain and boundary constraints. The deformation of microplastic grains for which σ_u and σ_ℓ are both stationary or both kinematic has been considered elsewhere (11). The presence of a K modelled behavior for σ_u has been ruled out as giving an unacceptable description of strain transients following a sudden change in cyclic stress (11), but the possibility of a K model of σ_ℓ and an S model of σ_u has not been examined.

For this study we model the latter situation by defining a composite material for the grain, assumed to experience the same local stress σ^ℓ in each element. Each of the two components ($i = 1,2$) is assigned a "plastic" modulus for plastic strain above its respective flow stress, giving a plastic strain increment

$$\Delta\varepsilon_p(i) = \frac{\Delta\sigma^\ell}{E_p(i)} \, . \qquad (1)$$

The strains in the two elements are summed; thus E_p contains a hidden dependence on both the strain hardening and the relative volume of the two components. The flow criteria are applied independently to each element in a numerical calculation (based on equations in Ref. 10) of the strains and stresses at each load reversal. This allows σ_ℓ to be defined according to a K model and σ_u to an S model status. (The complete formulation of this model will be discussed elsewhere.)

In addition we have considered a model describing a nonuniformly deforming grain represented by an interior enveloped by a shell of different mechanical properties near the grain boundary. The stress-strain behavior of such dual-domain systems has been described by Morris et al. (10). The constitutive equations for a dual-domain grain were implemented numerically for an arbitrary load sequence. In the following we use U and D to denote uniform and dual-domain grain models; the entry K/S refers to a K model of σ_ℓ and an S model of σ_u. For example, D-S/S is a dual-domain model with a stationary flow surface locus for both σ_ℓ and σ_u.

Results

Deformation in a 300 μm grain before σ_u develops during fatigue is examined in Fig. 1. The sample was cycled at ±270 MPa for 100 cycles and then the load was dropped to σ_a as shown in the insert of Fig. 1a. Measurement of W_o was made after 5 cycles at σ_a to allow for equilibrium of the local stress-strain response. Repetition of load shedding for multiple values of σ_a has been found most useful to determine the local mechanical properties of the grain (11). Material values were chosen for U-S/S and U-K/S models to fit the observed residual strains in Fig. 1a. However, for these same parameters, only the U-K/S model depicts the strain behavior for a sequence of tensile reloads to successively higher tensile maxima (σ_{max}) (Fig. 1b). The large increase in the σ_ℓ flow locus that occurs with a K model is necessary to prevent significant grain deformation on reloading.

After a few hundred fatigue cycles, σ_u appears (Fig. 2a). Residual strains measured during load shedding for fully reversed loading are again described by selection of appropriate material parameters for the two regions of flow for the U-K/S and U-S/S models. Using these coefficients, only the U-K/S model correctly represents

the increasing strain in response to a series of stress relaxation cycles around an increasingly more positive mean stress (σ_{mean}) (Fig. 2b). A kinematic increase of the σ_t flow locus suppresses the large internal strains that would develop with increasing mean stress. Another way this result might occur is if flow at the grain boundary lowered the maximum stress experienced by the grain interior. This possibility was examined using the dual-domain model (10). With appropriate selection of material properties for the boundary, the D-S/S model can almost mimic the behavior in Fig. 2b but, for the same material parameters, the representation of the behavior in fully reversed loading (Fig. 2a) is poor.

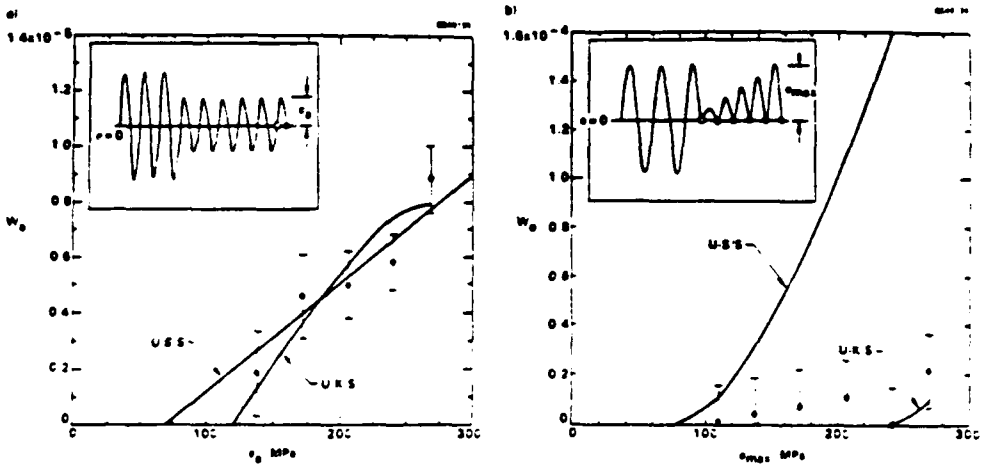

Fig. 1 Local strain behavior in a 300 μm grain after 100 cycles at ± 270 MPa. W_o is a residual strain measured at zero external load in the load sequence (solid circle), relative to an earlier point (open circle). a) As a function of the applied cyclic stress amplitude; b) for a series of loads of increasing tensile maximum σ_{max}, following unloading from 270 MPa.

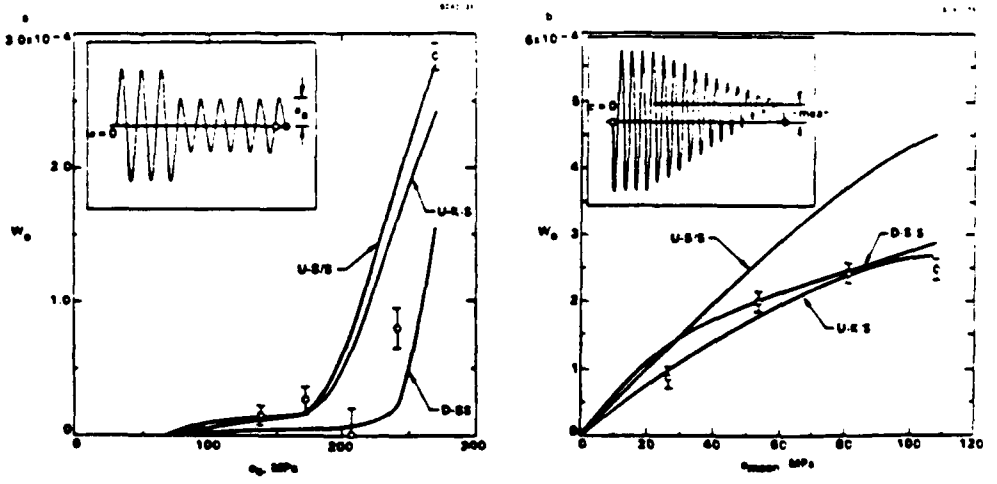

Fig. 2 Local strain behavior in a 300 μm grain after 250 cycles at ± 270 MPa. W_o is a residual strain measured at zero external load (solid circle) relative to an earlier point (open circle). a) As a function of the applied cyclic stress amplitude; b) following a stress envelope converging to a positive mean stress σ_{mean}, relative to an envelope collapsed to a zero mean.

Discussion

In a grain of monolithic properties, if σ_ℓ is less than σ_U for any loading sequence, then the relationship must hold for all sequences. This is simply because each region of flow in a monolithic material will be conditioned by particular levels of strain. To ensure this behavior in a two-stage yielding model, both the lower and upper flow stresses would have to be either stationary or kinematic. In contrast, the strain behavior of single grains we report for the mean stress and tensile reloading experiments is represented well only if, (1) the high strain hardening deformation found just above σ_ℓ occurs at a stress less than σ_U *in fully reversed loading*, and (2) if σ_ℓ is greater than σ_U after single large tensile excursions. It appears that for this to happen, σ_ℓ must be kinematic, σ_U stationary, and, further, that the grain must consist of a microscopic composite of material elements of two types, one having a flow stress σ_ℓ, the other σ_U. It also suffices to treat the deformation as uniform throughout the grain, so the individual composite subcomponents must be small compared to a 100 um gauge length. Since a stationary flow locus is tantamount to a large separation between dislocation pinning points, is σ_U then associated with banded slip? This would mean that onset of flow in the bands can require higher stresses than flow in the matrix (above σ_ℓ), an uncomfortable proposition except that flow in the bands involves much larger strains than in the matrix.

For Al 2219-T851 it is becoming clear that the relationship of σ_U to σ_ℓ in individual grains is extremely dependent on the prior load. It is, therefore, unavoidable that the local plastic strains in this material will be highly sensitive to the details of load sequence as well as to the amplitude range. With the assistance of a simple model depicting the way the material properties in the grain evolve with cumulative plasticity (14), it should now be possible to calculate how load sequence will effect the local strains, and hence the progress of fatigue crack initiation in isolated microplastic grains.

Summary

The complexities of the deformation of a large microplastic grain in Al 2219-T851 are revealed by local strain measurements made for external loading other than fully reversed. Two stages of flow are recognized, and a comparison with models of the deformation process suggests the likelihood that each takes place in a distinct subcomponent of the grain. Many of these elements must be intermingled to form a microscopic composite, as the deformation appears to be quasi-uniform over gauge lengths comparable to the grain size. One subcomponent, known to strain harden quickly with fatigue, is best described by a kinematic movement of the yield surface locus with prior loading, suggesting a reaction to short range back stresses in the grain. Deformation of the material is therefore extremely dependent on the prior load sequence. The second component dramatically strain softens with fatigue, and is best described by a "stationary" yield surface locus - suggestive of a long-ranged constraint of flow by grain boundaries. A physical representation of our model equations might be a matrix containing slip bands, although we know for the 2219 aluminum alloy that traditional persistent slip bands are not present. Nevertheless, the single uniform deformation model which incorporates both of these kinds of behavior provides an adequate description of the deformation of the isolated nonplastic grains in the 2219 aluminum alloy that are responsible for fatigue crack initiation.

Acknowledgement

This work was supported by the Naval Air Development Center under Contract No. N62269-86-C-0261. The experimental help of R.V. Inman at the Science Center is gratefully acknowledged.

References

1. A. Esin and W.J.D. Jones, "A Statistical Approach to Microplastic Strain in Metal," J. Strain Analysis 1 (1966), 415-421.

2. J. Polak and M. Klesnil, "The Hysteresis Loop, I. A Statistical Theory," Fat. Engng. Mater. and Struc. 5 (1982) 19-32.

3. M.R. James and W.L. Morris, "The Role of Microplastic Deformation in Fatigue Crack Initiation," Fatigue Mechanisms: Advances in Quantitative Measurement of Physical Damage, ASTM STP-811, Am. Soc. Testing and Materials, Philadelphia, PA, 46-70 (1983).

4. U.F. Kocks, "Kinetics of Nonuniform Deformation," Progress in Matls. Sci. Chalmers Anniversary Issue, ed. J.W. Christian et al., Pergamon Press, Oxford (1981), 185-241.

5. R.E. Stoltz and R.M. Pelloux, "The Bauschinger Effect, Monotoric and Cyclic Hardening in Precipitation Stengthened Aluminum Alloys," Work Hardening in Tension and Fatigue, ed. A.W. Thompson, AIME (1977) 224-229.

6. Y. Estrin and L.P. Kubin, "Local Strain Hardening and Nonuniformity of Plastic Deformation," Acta. Metall. 34 (1986) 2455-2464.

7. H. Mughrab., "Cyclic Plasticity of Matrix and Persistent Slip Bands in Fatigued Metals, Continuum Models of Discrete Systems, 4," Eds. O. Brulin and R.K.T. Hsieh, North-Holland Publ. Co. (1981) 241-157.

8. H. Mughrabi, "Dislocation Wall and Cell Structures and Long-Range Internal Stresses in Deformed Metal Crystals," Acta Metall. 31 (1983) 1367-1379.

9. H. Mughrabi, "On the Flow Stress of Deformed Metal Crystals Containing Heterogeneous Dislocation Distributions," S. Afr. J. Phys. 9 (1986) 62-68.

10. W.L. Morris, B.N. Cox and M.R. James, "Microplastic Surface Deformation of Al 2219-T851," Acta Metall. 35, (1986) 1055-1065.

11. B.N. Cox, W.L. Morris and M.R. James, "Two-Stage Microplastic Surface Deformation of Al 2219-T851," Acta Metall. 35 (1987), 1289-1300.

12. W.L. Morris, M.R. James and B.N. Cox, "The Evolution of Local Mechanical Properties of Al 2219-T851 During Fatigue," in Fatigue 87, 3rd Int. Conf. on Fatigue and Fatigue Thresholds, June 28-July 3, 1987, Charlottesville, VA, in press.

13. W.L. Morris and M.R. James, "Fundamental Characterization of Surface Microplasticity," Tech. Report, Contract No. DMR-8310652, NSF (Dec. 1984).

14. W.L. Morris, M.R. James and B.N. Cox, "A Phenomenological Model of the Mechanical Properties of Microplastic Grains During Fatigue," Maters. Sci. Engng. (1987), in press.

15. W.L. Morris, R.V. Inman and M.R. James, "Measurement of Fatigue Induced Surface Plasticity," J. Maters. Sci. 17 (1982) 1413-1419.

16. M.R. James and W.L. Morris, "The Fracture of Constituent Particles During Fatigue," Maters. Sci. Engng. 56 (1982) 63-71.

DISTRIBUTION LIST (Continued)

Dr. T. Hahn
The Pennsylvania State University
Dept. Engineering Science & Mechanics
227 Hammond Building
University Park, PA 16802

Vascar G. Harris
Dean, School of Engineering and Architecture
Tuskegee University
Tuskegee, AL 36088

Dr. D. Wilkins
University of Delaware
Mechanics & Aerospace Eng. Dept
Evans Hall
Newark, DE 19711

Dr. Frank Ko
Fibrous Materials Research Lab
Drexel University
31st and Chestnut Street
Philadelphia, PA 19104

DISTRIBUTION LIST (Continued)

University of Dayton Research Institute
Attn: Dr. J. Gallagher
300 College Park Avenue
Dayton, OH 45469 — 1 copy

University of Delaware
Attn: Dr. R. B. Pipes
Mechanics & Aerospace Eng. Dept.
Evans Hall
Newark, DE 19711 — 1 copy

University of Delaware
Attn: Dr. J. R. Vinson
Mechanics & Aerospace Eng. Dept.
Evans Hall
Newark, DE 19711 — 1 copy

University of Oklahoma
Attn: Dr. C. W. Bert
School of Aerospace, Mechanical
and Nuclear Engineering
Norman, OK 73019 — 1 copy

University of Wyoming
Attn: Dr. D. Adams
Laramie, WY 82071 — 1 copy

Villanova University
Attn: Dr. P. V. McLaughlin
Villanova, PA 19085 — 1 copy

Virginia Polytechnic Institue
Attn: Dr. K. Reifsnider
Blacksburg, VA 24061 — 1 copy

DISTRIBUTION LIST (Continued)

Georgia Institue of Technology
Attn: Prof. L. Rehfield
Atlanta, GA 30332 — 1 copy

HITCO
Attn: Mr. N. Myers
1600 West 135th Street
Gardena, CA 90249 — 1 copy

ITT Research Institute
Attn: Mr. K. Hofar
Chicago, IL 60616 — 1 copy

Technical Library
Kaman Aircraft Corp.
Bloomfield, CT 06002 — 1 copy

Lehigh University
Attn: Dr. G. C. Sih
Bethlehem, PA 18015 — 1 copy

Massachusetts Institute of
Technology
Attn: Dr. P. A. Lagace
77 Massachusetts Avenue
Cambridge, MA 02139 — 1 copy

Materials Sciences Corp.
Attn: Dr. B. W. Rosen
Spring House, PA 19477 — 1 copy

Purdue University
School of Aeronautics &
Astronautics
Attn: Dr. C. T. Sun
West Lafayette, IN 47907 — 1 copy

DISTRIBUTION LIST (Continued)

Anamet Laboratories
Attn: Dr. R. Arnold
3400 Investment Blvd.
Hayward, CA 94545-3811 — 1 copy

Battelle Columbus Laboratories
Metals and Ceramics Information Center
505 King Avenue
Columbus, OH 43201 — 1 copy

Bendix Product
Attn: Mr. R. V. Cervelli
Aerospace Division
South Bend, IN 46619 — 1 copy

Cabot Corporation
Billerica Research Center
Billerica, MA 01821 — 1 copy

Drexel University
Attn: Dr. P. C. Chou
32nd and Chestnut Streets
Philadelphia, PA 19103 — 1 copy

Drexel University
Attn: Dr. A. S. D. Wang
2nd and Chestnut Streets
Philadelphia, PA 19103 — 1 copy

E. I. DuPont Company
Attn: Mr. V. L Bertarelli
Chestnut Run Location, CR701
Wilmington, DE 19898 — 1 copy

Hercules Aerospace Division
Attn: Mr. D. Hug
P. O. Box 210
Rocket Center, WV 26726 — 1 copy

DISTRIBUTION LIST (Continued)

Northrop Corporation
Attn: Dr. Ratwani
One Northrop Avenue
Hawthorne, CA 90250 — 1 copy

Northrop Corporation
Attn: Mr. Alan Liu
One Northrop Avenue
Hawthorne, CA 90250 — 1 copy

Rockwell International Science Center
Attn: Dr. F. Morris
1049 Camino Dos Rios
Thousand Oaks, CA 91360 — 1 copy

University of Dayton Research Institute
Attn: Dr. Gallagher
300 College Park Avenue
Dayton, OH 45469 — 1 copy

LTV Aerospace and Defense Company
Attn: Dr. C. Dumesnil
P.O. Box 225907
Dallas, TX 75265-0003 — 1 copy

University of Oklahoma
School of Aerospace, Mechanical
and Nuclear Engineering
Attn: Dr. D. M. Egle
Norman, OK 78301 — 1 copy

DISTRIBUTION LIST (Continued)

LTV Aerospace and Defense Company
Attn: Mr. T. Gray
P.O. Box 225907
Dallas, TX 75265-0003 — 1 copy

Boeing Commercial Airplane Company
Attn: Mr. Porter
P.O. Box 3707
Seattle, WA 98124 — 1 copy

Fairchild Industries
Attn: Technical Library
Hagerstown, MD 21740 — 1 copy

Grumman Aerospace Corporation
Attn: Dr. H. Armen
South Oyster Bay Road
Bethpage, LI, NY 11714 — 1 copy

Lehigh University
Attn: Dr. Sih
Institute of Fracture & Solid Mechanics
Bethlehem, PA 18015 — 1 copy

Lehigh University
Attn: Dr. T. J. Delph
Institute of Fracture & Solid Mechanics
Bethlehem, PA 18015 — 1 copy

McDonnell Douglas Corporation
Attn: Mr. D. Rich
P. O. Box 516
St. Louis, MO 63166 — 1 copy

DISTRIBUTION LIST (Continued)

Northrop Corporation
Attn: Mr. A. Liu
One Northrop Avenue
Hawthorne, CA 90250 — 1 copy

Rockwell International Corporation
Attn: Mr. J. Chang
LA Division/International Airport
P.O. Box 92098
Los Angeles, CA 90009 — 1 copy

Sikorsky Aircraft
Attn: S. Garbo
110 N. Main Street
Stratford, CT 06622 — 1 copy

University of Illinois
College of Engineering
Attn: Professor D. Socie
Urbana, IL 61801 — 1 copy

University of Pennsylvania
Department of Mechanical Engineering
Attn: Dr. Burgers
111 Towne Bldg., D3
Philadelphia, PA 19104 — 1 copy

Rockwell International Corporation
Attn: Mr. F. Kaufman
4300 East Fifth Avenue
Columbus, OH 43216 — 1 copy

Rohr Corporation
Attn: Dr. F. Riel
Riverside, CA 92503 — 1 copy

Boeing Helicopter Company
Attn: C. Gunther
P.O. Box 16858
Philadelphia, PA 19142 — 1 copy

Douglas Aircraft Company
Attn: Mr. Luce (7-21)
3855 Lakewood Blvd.
Long Beach, CA 90846 — 1 copy

General Dynamics/Convair
Attn: Mr. G. Kruse
P.O. Box 80847
San Diego, CA 92138 — 1 copy

Grumman Aerospace Corporation
Attn: Dr. B. Leftheris
South Oyster Bay Road
Bethpage, LI, NY 11714 — 1 copy

Lehigh University
Attn: Prof. R. Wei
Institute of Fracture & Solid Mechanics
Bethlehem, PA 18015 — 1 copy

Lockheed Aeronautical Systems Co. - Georgia
Attn: Mr. T. Adams
86 S. Cobb Drive
Marietta, GA 30063 — 1 copy

Lockheed Aeronautical Systems Co. - Georgia
Attn: M. B. M. Shah
86 S. Cobb Drive
Marietta, GA 30063 — 1 copy

DISTRIBUTION LIST (Continued)

National Aeronautical & Space Adm
George C. Marshall Space Flight Ctr
Attn: Technical Library
Huntsville, AL 35812 — 1 copy

National Aeronautical & Space Adm
Lewis Research Center
Attn: Technical Library
Cleveland, OH 44135 — 1 copy

Air Force Systems Command
Attn: AFWAL/FDS
Wright Patterson Air Force Base
OH 45433 — 1 copy

Air Force Systems Command
Attn: AFWAL/FDSA
Wright Patterson Air Force Base
OH 45433 — 1 copy

Air Force Systems Command
Attn: AFWAL/FDSE
Wright Patterson Air Force Base
OH 45433 — 1 copy

ALCOA
ALCOA Labs
Attn: Mr. J. G. Kaufman
ALCOA Center, PA 15069 — 1 copy

Bell Helicopter Company
Textron Inc.
Attn: T. Haas
P.O. Box 482
Ft. Worth, TX 76101 — 1 copy

Boeing Helicopter Company
Attn: W. Kesack
P.O. Box 16858
Philadelphia, PA 19142 — 1 copy

DISTRIBUTION LIST (Continued)

General Dynamics Corporation
Attn: Dr. S. Manning
P.O. Box 748
Ft. Worth, TX 76101 — 1 copy

Grumman Aerospace Corporation
Attn: H. Eidenoff
South Oyster Bay Road
Bethpage, LI NY 11714 — 1 copy

Lockheed Aeronautical Systems Company
Attn: Mr. J. Ekvall/76-23, Bldg. 63
P. O. Box 551
Burbank, CA 91520 — 1 copy

Lockheed Aeronautical Systems Company
Attn: Mr. E. Walker/76-23, Bldg. 63
P.O. Box 551
Burbank, CA 91520 — 1 copy

McDonnell Aircraft Company
McDonnell Douglas Corporation
Attn: R. Pinckert
P.O. Box 516
St. Louis, MO 63166 — 1 copy

Federal Aviation Administration
800 Independence Avenue, SW
(Attn: Mr. J. Soderquist)
Washington, D.C. 20591 — 1 copy

National Aeronautics & Space Adm
Langley Research Center
Attn: Mr. C. E. Harris/MS188E
Hampton, VA 23365 — 1 copy

DISTRIBUTION LIST (Continued)

Army Materials Technology Laboratory
Attn: D. Oplinger/SLCMT-MS
Watertown, MA 02172-0001 — 1 copy

National Technical Information Center
U. S. Department of Commerce
Springfield, VA 221512 — 2 copy

Oklahoma City Air Logistics Center
Attn: MAQCP
Tinker Air Force Base
Oklahoma 73145 — 1 copy

United States Army
Research Office
Durham, NC 27701 — 1 copy

Defense Technical Information Center
Attn: Administrator
Building #5, Cameron Station
Alexandria, VA 22314 — 2 copies

U.S. Army R&D Center
Attn: STRBE-VC/L. Ryan
Fort Belvoir, VA 22060-5606 — 1 copy

Battelle Columbus Laboratories
Attn: Dr. B. Leis
505 King Avenue
Columbus, OH 43201 — 1 copy

Drexel University
Attn: Dr. Auerbuch
32nd and Chestnut Streets
Philadelphia, PA 19104 — 1 copy

DISTRIBUTION LIST (Continued)

Director
Naval Research Laboratory
Attn: Dr. R. Badaliance
Washington, DC 20375 — 1 copy

Sacramento Air Logistics Center
Attn: MANE/A. J. Hammond
McClellan Air Force Base
Sacramento, CA 95652 — 1 copy

Metals and Ceramics Information Ctr
Battelle Columbus Laboratories
505 King Avenue
Columbus, OH 43201 — 1 copy

Warner-Robbins Air Logistics Ctr
Attn: MMSRD/Mr. T. Christian
Robins Air Force Base
Georgia 30198 — 1 copy

Army Applied Technology Directorate
U.S. Army Aviation Research & Technology Activity
Attn: SAVRT-TY/H. Reddick
Fort Eustis, VA 23604-5577 — 1 copy

Ogden Air Logistics Center
Attn: MANCC
Hill Air Force Base
Utah 84055 — 1 copy

San Antonio Air Logistics Center
Attn: MMETM
Kelly Air Force Base
San Antonio, TX 78241 — 1 copy

NASA Headquarters
Attn: Dr. D. Mulville
OAST-Code RM
Washington, D.C. 20546 — 1 copy

Commander
Naval Air Engineering Center
Attn: Mr. F. Sinatra
Lakehurst, NJ 08733 — 1 copy

Commander
Naval Air Engineering Center
Attn: Mr. Neil Goodis
Lakehurst, NJ 08733 — 1 copy

Commanding Officer
Naval Aviation Depot
Attn: Technical Library
Marine Corps Air Station
Cherry Point, NC 28533-5030 — 1 copy

Commanding Officer
Naval Aviation Depot
Attn: Technical Library
North Island
San Diego, CA 92135 — 1 copy

Commander
Naval Aviation Depot Operations Center
Patuxent River, MD 20670 — 1 copy

Commander
David Taylor Research Center
Attn: Technical Library
Bethesda, MD 20034 — 1 copy

DISTRIBUTION LIST (Continued)

Commanding Officer
Naval Air Systems Command
Attn: AIR-530
Washington, D.C. 20361 — 3 copies

Commanding Officer
Naval Air Systems Command
Attn: AIR-5302
Washington, D.C. 20361 — 1 copy

Commanding Officer
Naval Air Systems Command
Attn: AIR-53021
Washington, D.C. 20361 — 1 copy

Commanding Officer
Naval Air Systems Command
Attn: AIR-53022
Washington, D.C. 20361 — 1 copy

Commanding Officer
Naval Air Systems Command
Attn: AIR-53023
Washington, D.C. 20361 — 1 copy

Federal Aviation Administration
Technical Center
Attn: Mr. L. Neri, Code ACT-330
Atlantic City, NJ 08405 — 1 copy

Federal Aviation Administration
Technical Center
Attn: Mr. M. Ciafa, Code ACT-330
Atlantic City, NJ 08405 — 1 copy

DISTRIBUTION LIST (Continued)

Commanding Officer
Naval Aviation Depot
Attn: Technical Library
Jacksonville, FL 32212 — 1 copy

Commanding Officer
Naval Aviation Depot
Attn: Technical Library
Pensacola, FL 32508 — 1 copy

Commander
Naval Post Graduate School
Attn: Prof. K. Challenger
Monterey, CA 95940 — 1 copy

Officer in Charge
David Taylor Research Center
Attn: 2814/T. Montemarano
Annapolis, MD 21402 — 1 copy

Naval Surface Weapons Center
White Oak Laboratory
Attn: Technical Library
Silver Spring, MD 20910 — 1 copy

Commanding Officer
Naval Air Systems Command
Attn: AIR-00D4
Washington, D.C. 20361 — 1 copy

Commanding Officer
Naval Air Systems Command
Attn: AIR-931B
Washington, D.C. 20361 — 1 copy

NAVAIRDEVCEN
Attn: Code 8131
Warminster, PA 18974-5000 — 2 copies

DISTRIBUTION LIST
REPORT NO. NADC-89044-60

Commander
Naval Air Test Center
Attn: Dr. J. Hoeg
Patuxent River, MD 20670 — 1 copy

Commanding Officer
Naval Aviation Depot
Attn: Technical Library
Alameda, CA 94501 — 1 copy

Commanding Officer
Naval Aviation Depot
Attn: Mr. H. Stokley
Norfolk, VA 23511-5899 — 1 copy

Commander
Naval Weapons Center
Attn: J. Morrow, Code 338
China Lake, CA 93555 — 1 copy

Naval Sea Systems Command
Attn: SEA-05R
Washington, D.C. 20362-5101 — 1 copy

Office of Naval Research
Attn: Dr. Rajapakse, Code 11325M
800 North Quincy Street
Arlington, VA 22217 — 1 copy

Office of Naval Technology
Attn: Capt. K. Cox, ONT-21
800 North Quincy Street
Arlington, VA 22217 — 1 copy

Center for Naval Analyses
4401 Font Avenue
P.O. Box 16268
Alexandria, VA 22302-0268 — 1 copy